ISSN 2409-5613 (print)
ISSN 2411-1414 (online)

Chimica Techno Acta

2018. Vol. 5. N 3

cta.urfu.ru

Founded by Ural Federal University named after the first President of Russia B. N. Yeltsin
19, Mira St., Ekaterinburg, 620002, Russia

Chimica Techno Acta

2018 | Vol. 5 | № 3

Scientific and Technical Journal
Established in 2014
Published four times per year

Учредитель — Уральский федеральный университет имени первого Президента России Б. Н. Ельцина
620002, Россия, Екатеринбург, ул. Мира, 19

Chimica Techno Acta

2018 | Vol. 5 | № 3

Научно-технический журнал
Журнал основан в 2014 г.
Выходит четыре раза в год

Graphical Abstracts

CONTENTS/СОДЕРЖАНИЕ

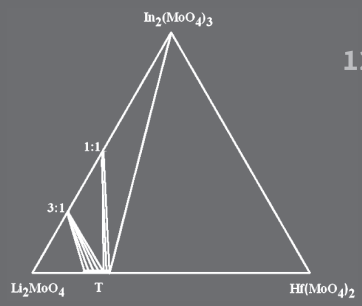

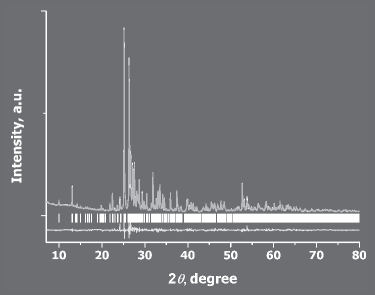

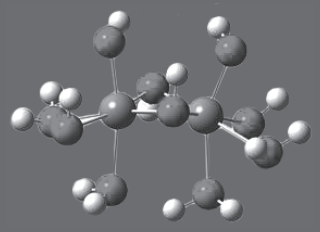

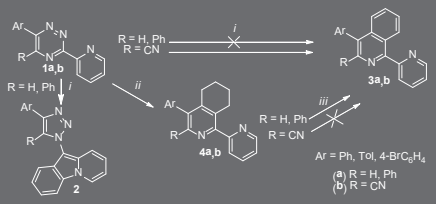

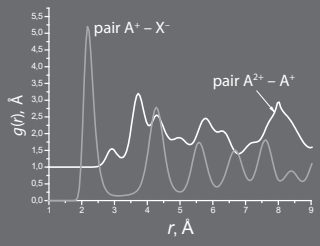

Chimica Techno Acta
2018. Vol. 5, № 3

Bazarova J. G., Tushinova Yu. L., Grossman V. G.,
Bazarova Ts. T., Bazarov B. G., Kurbatov R. V.
Chimica Techno Acta. 2018. Vol. 5, No. 3. P. 126–131.
ISSN 2409–5613

DOI: 10.15826/chimtech.2018.5.3.01

J. G. Bazarova*, Yu. L. Tushinova, V. G. Grossman, Ts. T. Bazarova, B. G. Bazarov, R. V. Kurbatov

Baikal Institute of Nature Management
Siberian Branch of the Russian Academy of Sciences
8 Sakh'yanovoi St., Ulan-Ude, Buryat Republic, Russian Federation
**E-mail: jbaz@binm.ru*

Phase relations in the Me_2MoO_4–$In_2(MoO_4)_3$–$Hf(MoO_4)_2$ systems, where Me = Li, K, Tl, Rb, Cs

The Me_2MoO_4–$In_2(MoO_4)_3$–$Hf(MoO_4)_2$ systems where Me = Li, K, Tl, Rb, Cs were studied in the subsolidus region using an X-ray powder diffraction. Quasi-binary joins were revealed, and triangulation carried out. The formation of ternary molybdates $Me_5InHf(MoO_4)_6$ for Me = K, Tl, Rb, Cs and $Me_2InHf_2(MoO_4)_{6.5}$ for Me = Rb, Cs was established.

Keywords: phase relations, triangulation, solid-phase reactions, X-ray phase diffraction, molybdates.

Received: 26.09.2018. Accepted: 12.10.2018. Published: 31.10.2018.

Introduction

Ternary molybdates attract attention due to their catalytic and ionexchange properties and the diversity of their crystal structures. The MoO_6 octahedra are usually highly distorted because of the relatively small effective radius of the Mo^{6+} ion in the oxygen environment, which is favorable for the formation of low-symmetry crystal structures.

Systematic studies of multicomponent systems allow obtaining the large amount of data which make it possible to identify regularities of the phase formation in related systems. In our previous works, the phase equilibria in the Me_2MoO_4–$R_2(MoO_4)_3$–$Hf(MoO_4)_2$ (Me = Rb, Cs; R — trivalent metals) systems were studied [1, 2].

The purpose of this work was to establish the phase formation in the Me_2MoO_4–$In_2(MoO_4)_3$–Hf $(MoO_4)_2$ systems where Me = Li, K, Tl, Rb, Cs.

Experimental

Subsolidus phase relations in the Me_2MoO_4–$In_2(MoO_4)_3$–$Hf(MoO_4)_2$ (Me = Li, K, Tl, Rb, Cs) systems were studied within the temperature range 450–550 °C using the intersecting joins method.

The correspondent molybdates of lithium, potassium, thallium, rubidium, cesium, indium and hafnium were used as starting components for studying the phase equilibria in the Me_2MoO_4–$In_2(MoO_4)_3$–$Hf(MoO_4)_2$ (Me = Li, K, Tl, Rb, Cs) systems. In order to avoid MoO_3 losses due to the sublimation, annealing was started at 400 °C. Synthesis of thal-

lium molybdate Tl_2MoO_4 was performed according to the following reaction:

$$Tl_2O_3+MoO_3 \rightarrow Tl_2MoO_4+O_2\uparrow$$

while the temperature was gradually increased in the range of 400–550 °C for 50 h.

Binary alkali molybdates Me_2MoO_4 (Me = Li, K, Rb, Cs) were synthesized by the solid-state reaction using stoichiometric mixtures of alkali carbonates or nitrates with molybdenum trioxide for 80–100 h.

Hafnium molybdate was prepared by step annealing of stoichiometric mixtures of HfO_2 and MoO_3 within the temperature range 400–700 °C for 100–150 h. Indium molybdate was synthesized from indium oxide (III) In_2O_3 and molybdenum oxide (VI) MoO_3 by solid-state reaction at 500–700 °C.

X-ray powder diffraction (XRD) measurements were performed using a Bruker D8 Advance diffractometer (Bragg — Brentano geometry, Cu Kα radiation, secondary monochromator, maximum angle 2θ = 100°, scan step 0.02°).

Results and discussion

Information about the known phases in the side quasi-binary systems, which formed studied quasi-ternary Me_2MoO_4–$In_2(MoO_4)_3$–$Hf(MoO_4)_2$ (Me = Li, K, Tl, Rb, Cs) systems, required for triangulation, was taken from the literature. According to Solodovnikov et al. [3], the Li_2MoO_4–$Hf(MoO_4)_2$ system contains a lithium hafnium molybdate $Li_{10-4x}Hf_{2+x}(MoO_4)_9$ ($0.21 \leq x \leq 0.68$). Two types of double molybdates, $Me_8Hf(MoO_4)_6$ and $Me_2Hf(MoO_4)_3$ (Me = K, Tl, Rb, Cs), are formed inside the Me_2MoO_4–$Hf(MoO_4)_2$ systems [4–6]. An existence of the double molybdates, namely: $Li_3In(MoO_4)_3$, $MeIn(MoO_4)_2$ (Me = Li, K, Tl, Rb, Cs), and $Me_5In(MoO_4)_4$ (Me = Tl, Rb) was confirmed in the Me_2MoO_4–$In_2(MoO_4)_3$ systems [7–10]. No intermediate compounds were found inside the $In_2(MoO_4)_3$–$Hf(MoO_4)_2$ system [11].

Taking into account the aforementioned data, the phase formation in the Me_2MoO_4–$In_2(MoO_4)_3$–$Hf(MoO_4)_2$ (Me = Li, K, Tl, Rb, Cs) systems were studied by means of so-called "intersection joins method". Within this approach, we analyzed the XRD results for the samples representing the intersection points of the joins that connect the starting components and phases inside the quasi-binary systems. This makes it possible to establish the quasi-binary joins and, as a result, to implement the triangulation of the system. Since the phase relations in the K_2MoO_4–$In_2(MoO_4)_3$ and Cs_2MoO_4–$In_2(MoO_4)_3$ systems enriched by either potassium molybdate or by cesium molybdate were found to be non-quasibinary, the studies of the Me_2MoO_4–$In_2(MoO_4)_3$–$Hf(MoO_4)_2$ (Me = K, Cs) systems were limited to the $Hf(MoO_4)_2$–$Me_8Hf(MoO_4)_6$–$MeIn(MoO_4)_2$–$In_2(MoO_4)_3$ (Me = K, Cs) regions. The results obtained are presented in Fig. 1 and Fig. 2.

All systems under investigation can be categorized into three groups depending on the phase compositions of the binary subsystems and triple molybdates. The first group comprises the Li_2MoO_4–$In_2(MoO_4)_3$–$Hf(MoO_4)_2$ simple eutectic system without intermediate phases inside. The second group consists of the Me_2MoO_4–$In_2(MoO_4)_3$–$Hf(MoO_4)_2$ systems where Me = K and Tl, with one intermediate phase, denoted in Fig. 1 as S — $Me_5InHf(MoO_4)_6$ (5:1:2 mole ratio). The third group includes the Me_2MoO_4–

$In_2(MoO_4)_3$–$Hf(MoO_4)_2$ systems where (Me = Rb, Cs), with two intermediate phases: S_1 – $Me_5InHf(MoO_4)_6$ (5:1:2 mole ratio) and S_2 — $Me_2InHf(MoO_4)_6$ (2:1:4 mole ratio).

Single-phase samples of $Me_5InHf(MoO_4)_6$ (Me = K, Tl, Rb, Cs)

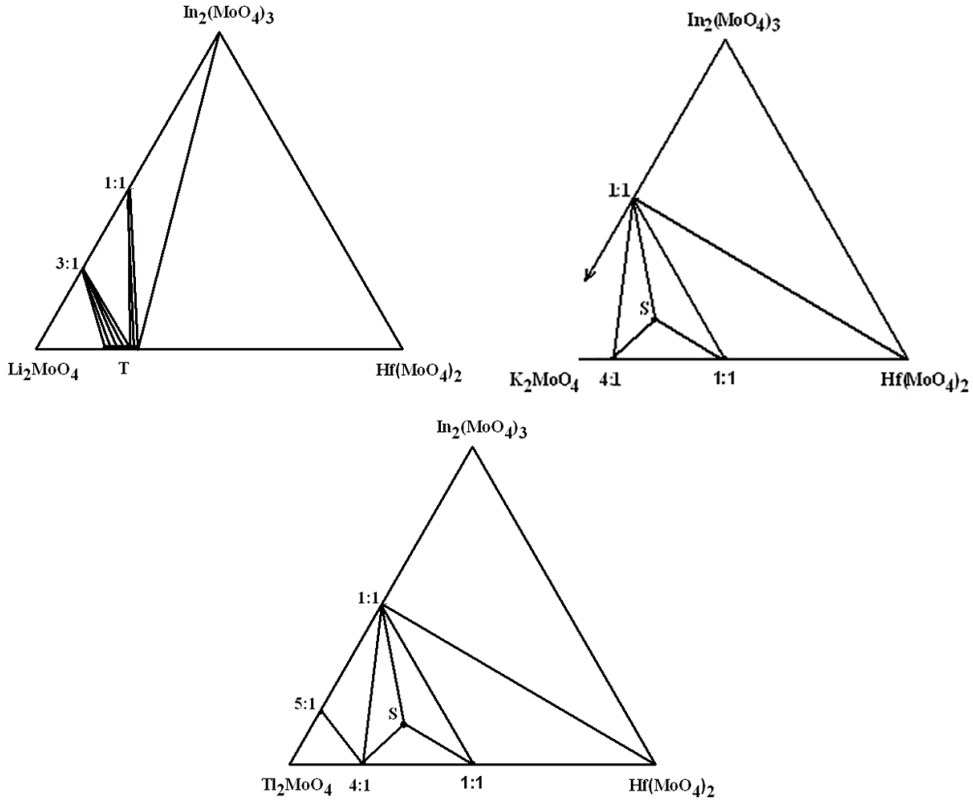

Fig. 1. Subsolidus phase relations in the Me_2MoO_4–$In_2(MoO_4)_3$–Hf $(MoO_4)_2$ (Me = Li, K, Tl) systems: S – $Me_5InHf(MoO_4)_6$ (5:1:2 mole ratio)

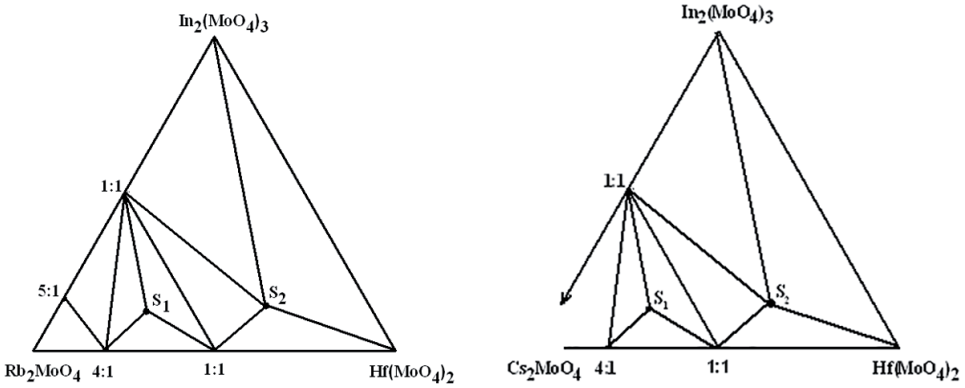

Fig. 2. Subsolidus phase relations in the Me_2MoO_4–$In_2(MoO_4)_3$–$Hf(MoO_4)_2$ (Me = Rb, Cs) systems: S_1 – Me_5InHf $(MoO_4)_6$ (5:1:2 mole ratio); S_2 — $Me_2InHf(MoO_4)_6$ (2:1:4 mole ratio)

and $Me_2InHf(MoO_4)_6$ (Me = Rb, Cs) were prepared by annealing the stoichiometric mixtures of quasi-binary molybdates at 450–600 °C for 80–100 h. Ternary molybdates $Me_5InHf(MoO_4)_6$ (Me = K, Tl, Rb, Cs) and $Me_2InHf(MoO_4)_6$ (Me = Rb, Cs) are insoluble in water and usual organic solvents, but were found to be soluble in HCl aqueous solution.

The ternary molybdates $Me_5InHf(MoO_4)_6$ (Me = K, Tl, Rb, Cs) are located inside the triangle that is formed by the double molybdates $MeR(MoO_4)_2$, $Me_8Hf(MoO_4)_6$ and $Me_2Hf(MoO_4)_3$ in its vertices.

The number of phases formed in the systems under consideration increases as the size of the singly charged alkali cation increases. The only exception is thallium-containing system. A distinctive feature of thallium is that it combines properties of alkali metals, such as potassium, rubidium, and cesium, together with those related to heavy metals, such as copper (I), silver, and lead [12].

The single crystals of new ternary potassium indium hafnium molybdate $K_5InHf(MoO_4)_6$ were grown by fluxed-melt crystallization with spontaneous nucleation [13]. The composition and crystal structure of as-grown single crystals were refined using X-ray diffraction data (a CAD-4 automated diffractometer, Mo Kα radiation, 1498 reflections, R = 0.0252). The crystal structure was solved as trigonal with the following unit cell parameters: a = 10.564 (1) Å, c = 37.632 (4) Å, V = 3637.0 (6) Å^3, Z = 6, space group $R\bar{3}c$. A three-dimensional mixed framework of the structure is formed by Mo tetrahedra and two independent (In, Hf) octahedra, which are connected through the shared vertices. Two types of potassium atoms occupy the large voids within the framework. The distribution of In^{3+} and Hf^{4+} cations over two different sites was refined as presented in the caption for Fig. 3.

Fig. 4 illustrates the IR and Raman spectra for the triple rubidium indium

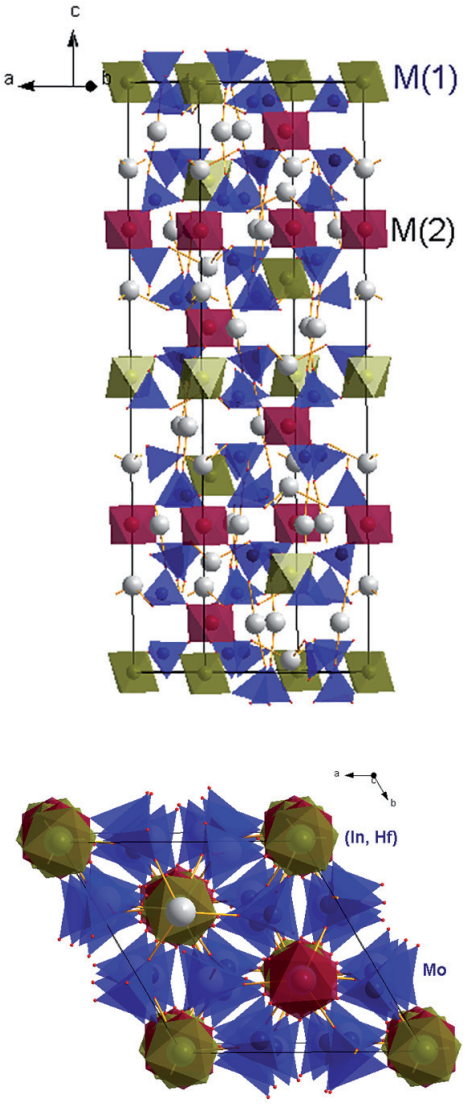

Fig. 3. Mixed framework of MoO_4 tetrahedra (blue color) and two types of octahedra $(In, Hf)O_6$ in the $K_5InHf(MoO_4)_6$ crystal structure. M(1) = 0.413(1)Hf + 0.587(1)In (olive color); M(2) = 0.587(1)Hf + 0.413(1)In (burgundy color)

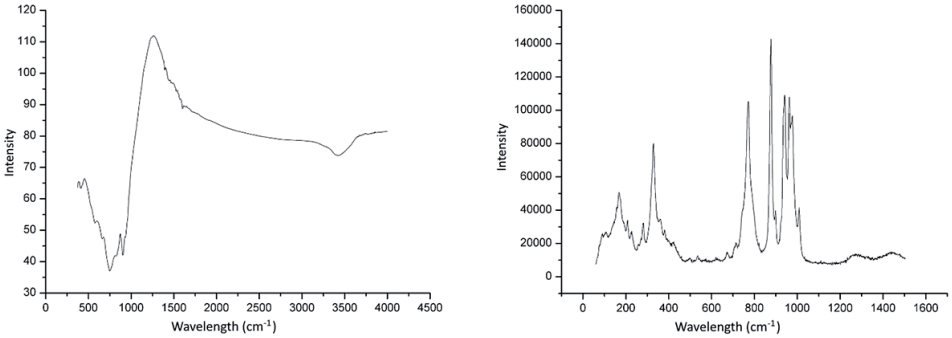

Fig. 4. IR and Raman spectra of $Rb_2InHf_2(MoO_4)_{6.5}$

hafnium molybdate $Rb_2InHf_2(MoO_4)_{6.5}$. Since the oscillation frequencies in the IR and Raman spectra differ from each other, one can assume that ternary molybdate $Rb_2InHf_2(MoO_4)_{6.5}$ and its analogues are centrosymmetric.

Conclusions

The phase equilibria in quasi-ternary salt systems were studied; six new compounds were identified inside the studied systems. The phase relations in the Me_2MoO_4–$In_2(MoO_4)_3$–$Hf(MoO_4)_2$ (Me = Li, K, Tl, Rb, Cs) systems are influenced by the size factor and the nature of the singly charged alkali cation.

Acknowledgements

The work was carried out according to the state assignment BINM SB RAS (project no. 0339-2016-0007) and RFBR, grants Nos. 18-03-00799.

References

1. Bazarov BG, Klevtsova RF, Bazarova TsT, Glinskaya LA, Fedorov KN, Tsyrendorzhieva AD, Chimitova OD, Bazarova JG. Phase equilibria in the systems Rb_2MoO_4–$R_2(MoO_4)_3$–$Hf(MoO_4)_2$ (R = Al, In, Sc, Fe (III)) and the crystal structure of double molybdate $RbFe(MoO_4)_2$. *Russ J Inorg Chem*. 2006;51(7):1111–5. DOI: 10.1134/S0036023606070151.
2. Bazarova JG, Tushinova YL, Bazarov BG, Oyun BE, Angarhayev JD. Phase equilibrium in the systems Cs_2MoO_4–$R_2(MoO_4)_{(3)}$–$Hf(MoO_4)_{(2)}$ (R = Al, Cr, Fe, Bi, La-Lu). *Izvestiya vuzov prikladnaya khimiya i biotekhnologiya*. 2018;8(2):19–28. DOI: 10.21285/2227-2925-2018-8-2-19-28.
3. Solodovnikov SF, Balsanova LV, Bazarov BG, Zolotova ES, Bazarova ZhG. Phase formation in the Rb_2MoO_4–Li_2MoO_4–$Hf(MoO_4)_2$ system and the crystal structure of $Rb_5(Li_{1/3}Hf_{5/3})(MoO_4)_6$. *Russ J Inorg Chem*. 2003;48(7):604–14.
4. Bazarov BG, Klevtsova RF, Bazarova TsT, Glinskaya LA, Fedorov KN, Bazarova ZhG, Chimitova OD. Systems Tl_2MoO_4–$E(MoO_4)_2$, where E = Zr or Hf, and the crystal structure of $Tl_8Hf(MoO_4)_6$. *Russ J Inorg Chem*. 2006;51(5):794–9. DOI: 10.1134/S0036023606050184.

5. Trunov VK, Efremov VA, Velikodny YuA. Crystal chemistry and properties of double molybdates and tungstates. Leningrad: Nauka; 1986. 173 p. Russian.
6. Klevtsova RF, Zolotova ES, Glinskaya LA, Klevtsov PV. Synthesis of double zirconium and hafnium molybdenum with cesium and crystal structure $Cs_8Zr(MoO_4)$. *Kristallografiya*. 1980;25 (5):972.
7. Velikodny YuA, Trunov VK, Markelova NI. Reaction of alkali metal molybdates (Li, Na, K) with indium molybdate. *Russ J Inorg. Chem*. 1970;15(11):1587–1592.
8. Velikodny YuA, Efremov VA, Trunov VK. Crystal structure of high temperature α-$LiIn(MoO_4)_2$. *Kristallografiya*. 1980;25(1):165–8.
9. Khaikina EG. Synthesis, peculiarities of phase formation and the structure of double and triple-molibdate one — and trivalent metals [dissertation]. Novosibirsk (Russia); 2008. 39 p.
10. Pleskov MY, Morozov VA, Lazoryak BI, Zhizhin MG, Burdakova IB, Khalbaeva KM, Tsyrenova GD, Khaikina EG. Structures of double molybdates $TlR(MoO_4)_2$ (R = In, Sc, Fe, Cr, Al). *Russ J Inorg Chem*. 2005;4 (50):604–14.
11. Tushinova YuL, Bazarova ZhG, Archincheyeva SI. Abstracts of the reports — Ulan-Ude: Publishing house of BSC SB RAS. 2002:90–91. Russian.
12. Nekrasov BN. Principles of General Chemistry. Moscow: Khimiya; 1967. 216 p. Russian.
13. Bazarov BG, Klevtsova RF, Bazarova TT, Glinskaya LA, Fedorov KN, Bazarova ZG. Synthesis and crystal structure of triple molybdate $K_5InHf(MoO_4)_6$. *Russ J Inorg Chem*. 2005;50(8):1146–9.

Kotova I. Yu., Savina A. A., Vandysheva A. I.,
Belov D. A., Stefanovich S. Yu.
Chimica Techno Acta. 2018. Vol. 5, No. 3. P. 132–143.
ISSN 2409–5613

DOI: 10.15826/chimtech.2018.5.3.02

I. Yu. Kotova[a], A. A. Savina[a]*,
A. I. Vandysheva[b], D. A. Belov[c], S. Yu. Stefanovich[c]

[a]Baikal Institute of Nature Management, Siberian Branch,
Russian Academy of Sciences,
6 Sakh'yanova St., Ulan-Ude, 670047, Buryat Republic, Russian Federation
[b]Buryat State University,
24a Smolin St., Ulan-Ude, 670000, Buryat Republic, Russian Federation
[c]Lomonosov Moscow State University,
Leninskie Gory, 1, Moscow 119991, Russian Federation
**E-mail: alex551112@mail.ru*

Synthesis, crystal structure and electrophysical properties of triple molybdates containing silver, gallium and divalent metals

A possibility of the triple molybdates formation with both NASICON-like and $NaMg_3In(MoO_4)_5$ structures in the Ag_2MoO_4–$AMoO_4$–$Ga_2(MoO_4)_3$ (A = Mn, Co, Zn, Ni) systems was studied by powder X-ray diffraction analysis. It was established that NASICON-like phases $Ag_{1-x}A_{1-x}Ga_{1+x}(MoO_4)_3$ are not formed. The triple molybdates $AgA_3Ga(MoO_4)_5$ (A = Mn, Co, Zn) isostructural to triclinic $NaMg_3In(MoO_4)_5$ (sp. gr. $P\bar{1}$, Z = 2) were synthesized and characterized. The structure of the obtained compounds was refined for $AgZn_3Ga(MoO_4)_5$ according to the powder data by the Rietveld method. The structure consists of MoO_4 tetrahedra, couples of edge-shared $M(1)O_6$ octahedra, and trimers of edge-shared $M(2)O_6$–, $M(3)_6$– and $M(4)O_6$ octahedra, which are linked by the common vertices to form a 3D framework. High-temperature conductivity measurements revealed that the conductivity of $AgMn_3Ga(MoO_4)_5$ at 500 °C reaches 10^{-2} S/cm, which is close to one of the known NASICON-type ionic conductors.

Keywords: triple molybdates; silver; gallium; solid-state synthesis; powder X-ray diffraction; Rietveld refinement; ionic conductivity.

Received: 10.10.2018. Accepted: 22.10.2018. Published: 31.10.2018.

Introduction

A synthesis and studying of complex oxide compounds, the development of new materials with functionally significant properties based on those are among the main areas of the materials science. An important place in the study and obtaining of new phases with valuable physicochemical properties belongs to molybdates, in particular triple ones, which are among the fastest-growing groups of complex oxide compounds containing a tetrahedral anion and three different cations. One of the largest families of these compounds is molybdates containing 1-, 2- and 3-charged cations. In particular, silver-containing NASICON-like phases

$Ag_{1-x}A_{1-x}R_{1+x}(MoO_4)_3$ (A = Mg Co, R = Al; A = Mg, R = In) with different homogeneity range and triclinic $AgA_3R(MoO_4)_5$ (A = Mg, R = Cr, Fe, Ga; A = Mn, R = Al, Cr, Fe, Sc, In) having high ionic conductivity (10^{-3}–10^{-2} S/cm) are of interest. For a number of phases: $AgMg_3R(MoO_4)_5$ (R = Cr, Fe), $AgMn^{II}_3$ $(Mn^{III}_{0.26}Al_{0.74})(MoO_4)_5$, $Ag_{0.90}Al_{1.06}Co_{2.94}(MoO_4)_5$ and $AgFe^{II}_3Fe^{III}(MoO_4)_5$ single crystals were obtained and their crystal structures were determined [1–9].

The purpose of this work is to study the possibility of forming triple molybdates $Ag_{1-x}A_{1-x}Ga_{1+x}(MoO_4)_3$ and $AgA_3Ga(MoO_4)_5$ (A = Mn, Co, Zn, Ni) and investigate crystal structure and electrophysical properties of the obtained compounds.

Experimental

The initial materials were simple molybdates of silver, manganese, cobalt, zinc, nickel, MoO_3 and Ga_2O_3 (reagent grade).

Ag_2MoO_4 and molybdates of divalent metals were obtained by the step annealing of stoichiometric mixtures of $AgNO_3$ (analytical grade), MnO, $Co(NO_3)_2{\cdot}6H_2O$, ZnO, MoO_3 (all chemically pure), NiO (reagent grade) at 350–450 °C (Ag_2MoO_4), 400–750 °C ($MnMoO_4$), 300–700 °C ($CoMoO_4$), 500–700 °C ($ZnMoO_4$), 450–750 °C ($NiMoO_4$) in the air with intermittent grindings every 15 hours for better sample homogenization. Power X-ray diffraction (PXRD) patterns of the prepared compounds do not contain reflections of starting or impurity phases. PXRD and thermal characteristics of all prepared compounds agree well with corresponding data reported in [10–15].

Sample compositions $Ag_{1-x}A_{1-x}Ga_{1+x}(MoO_4)_3$ ($0 \le x \le 0.7$, $\Delta x = 0.1$) and $AgA_3Ga(MoO_4)_5$ were prepared by the annealing of appropriate stoichiometric mixtures of Ag_2MoO_4, $AMoO_4$, MoO_3 and Ga_2O_3. The initial mixtures were annealed starting at 300 °C followed by raising the temperature by 20–50 °C (in some cases, 5–10 °C) with intermittent grindings every 20–30 hours for sample homogenization. The calcination time at each temperature was 30–70 h. The phase composition of the obtained products was controlled by the PXRD analysis before each increasing of the annealing temperature.

PXRD patterns were collected at room temperature on a Bruker D8 ADVANCE diffractometer using Cu Kα radiation in the 2θ range from 5° to 100° with a step of 0.02076°. Possible impurity phases were checked by comparing their PXRD patterns with those in the Powder Diffraction File. The crystal structure refinement was carried out with the GSAS [16] program suite using PXRD data. Lattice parameters and individual scale factors were established, and five common peak-shape parameters of the pseudo-Voigt function (No. 2), one asymmetry parameter and one parameter for the zero-point correction were used to describe the powder patterns. The background level was described by a combination of 15-order Chebyshev polynomials. Isotropic displacement parameters (Uiso) were refined, and grouped by chemical similarity by used constrains.

Thermoanalytic studies were carried out on a STA 449 F1 Jupiter NETZSCH thermoanalyser (Pt crucible, heating rate of 10 °C/min in Ar stream).

Ceramic disks for dielectric investigations were prepared by the calcination of pressed powder at 600 °C for 2 h. The disks were of 9–10 mm in diameter and

1–2 mm thick, the electrodes were deposited by painting the disk bases with colloid platinum followed by subsequent one hour annealing at about 580 °C. The direct current (DC) electric conductivity was measured with a V7–38 microammeter. To study the ion transfer, electrical conductivity was measured on an alternating current (AC) by the two-contact method in the frequency range 1 Hz–1 MHz in the temperature range 25–560 °C at the rate of 4 °C/min at both heating and cooling using a Novocontrol Beta-N impedance analyzer. The activation energy of electrical conductivity was calculated from the slope of the straight lines corresponding to the Arrhenius dependence in $\lg(\sigma T) - (10^3/T)$ coordinates.

Results and discussion

PXRD characteristics

The presence of NASICON-like phases in the Ag_2MoO_4–$AMoO_4$–$Ga_2(MoO_4)_3$ systems was determined according to PXRD analysis of samples $Ag_{1-x}A_{1-x}Ga_{1+x}(MoO_4)_3$ ($0 \le x \le 0.7$, $\Delta x = 0.1$) which were annealed in the temperature range from 300 °C to melting point. The final annealed temperature was 550–700 °C and depended on both the composition of the reaction mixtures and the nature of the divalent metal. It was established that, despite the close values of the Al^{3+} (0.53) and Ga^{3+} (0.62 Å [17]) radii, gallium containing triple molybdates with NASICON-like structure, apparently, do not exist. All our attempts to obtain rhombohedral phases $Ag_{1-x}A_{1-x}Ga_{1+x}(MoO_4)_3$ by solid state synthesis did not lead to a positive result, probably this is due to the low reactivity of gallium in the molybdate systems. Thus, the simple gallium molybdate $Ga_2(MoO_4)_3$ has not yet been obtained by ceramic technology, and only recently it was synthesized by the sol-gel method [18]. Besides, silver-gallium double molybdate is not synthesized either by ceramic technology or by co-precipitation. In [19] this compound was obtained by the calcining of mixtures of $AgNO_3$, Ga_2O_3, MoO_3 (in ratio 2:1:4) at 350–400 °C for 8–10 h, followed by cooling, homogenization, and the repeated 12–20 hours annealing at 500–550 °C, but the PXRD data of the product are not given by the authors. It should be noted that in none of the later publications (including those of the same authors) additional information about this compound was found.

At the same time, in the Ag_2MoO_4–$AMoO_4$–$Ga_2(MoO_4)_3$ systems triple molybdates of composition $AgA_3Ga(MoO_4)_5$ were found. These compounds were synthesized by the solid-state reactions at 550–600 °C (A = Mn), 540–550 °C (A = Zn), 500–530 °C (A = Co) for 80–100 h. However, nickel-containing compound was not obtained in the single-phase state, even after sintering at temperatures as high as 600–650 °C for 250–300 hours. This may be due to the smallest radius of Ni^{2+} cation (0.69 Å for CN = 6 [17]) in the studied series of simple molybdates of divalent metals.

The triple molybdates $AgA_3Ga(MoO_4)_5$ (A = Zn, Mn, Co) were found to melt incongruently at temperatures of 644, 727, and 739 °C, respectively.

The powder XRD patterns of as-prepared single-phase compounds $AgA_3Ga(MoO_4)_5$ are similar and show that these oxides are isostructural to triclinic $NaMg_3In(MoO_4)_5$ (sp. gr. $P\bar{1}$, Z = 2) [20]. The diffractograms of the $AgA_3Ga(MoO_4)_5$ (A = Mn, Co, Zn) were indexed with taking into account our data obtained earlier in the course of single-crystal structure de-

termination of $AgMg_3R(MoO_4)_5$, R = Fe, Cr [7]. The result of indexing the PXRD patterns for $AgA_3Ga(MoO_4)_5$ (A = Mn, Co, Zn) are given in Table 1. Unit-cell parameters are listed in Table 2.

Crystal structure of $AgZn_3Ga(MoO_4)_5$

The crystal structure of $AgZn_3Ga(MoO_4)_5$ was refined according to the Rietveld method [21], starting with the atomic coordinates of $AgMg_3Fe(MoO_4)_5$ structure [7]. Crystal data, data collection and structure refinement details are summarized in Table 3. Experimental, theoretical, and difference PXRD patterns for the $AgZn_3Ga(MoO_4)_5$ are shown in Figure 1. The fractional

Table 1

The calculated and observed values of PXRD data for $AgA_3Ga(MoO_4)_5$ (A = Mn, Zn, Co)

h	k	l	$AgMn_3Ga(MoO_4)_5$			$AgZn_3Ga(MoO_4)_5$			$AgCo_3Ga(MoO_4)_5$		
			I/I_0	$2\theta_{obs.}$,°	$2\theta_{cal.}$,°	I/I_0	$2\theta_{obs.}$,°	$2\theta_{cal.}$,°	I/I_0	$2\theta_{obs.}$,°	$2\theta_{cal.}$,°
0	0	2	3	9.861	9.850	2	9.981	9.991	2	10.006	10.019
0	1	0	1	12.782	12.767	1	12.954	12.945	1L	12.956	12.943
1	0	0	9	12.903	12.894	9	13.058	13.064	9	13.112	13.108
0	1	1							1L	13.769	13.750
1	0	1	1L	13.654	13.637	1	13.778	13.808	1L	13.853	13.849
0	−1	1				1L	14.021	13.998	1L	14.005	14.017
−1	0	1	1L	13.974	13.977	2	14.170	14.175	1	14.231	14.226
0	0	3	1L	14.805	14.798	1	15.010	15.011	1L	15.061	15.052
1	0	2	1	15.924	15.959	1L	16.154	16.157	1	16.177	16.200
0	−1	2	1L	16.388	16.393	1L	16.577	16.576	1	16.625	16.619
−1	0	2	1L	16.529	16.538	1L	16.799	16.783	1L	16.819	16.844
1	1	1				1L	17.079	17.075			
−1	−1	1				1L	17.541	17.562	1L	17.596	17.610
1	1	2	1L	18.728	18.728						
1	0	3	1L	19.304	19.310						
−1	−1	2	2	19.638	19.630	3	19.826	19.822	3	19.892	19.891
0	0	4	1	19.780	19.774				1L	20.127	20.115
−1	1	0			19.792	1L	20.115	20.122			20.154
−1	0	3	1L	20.025	20.033	1L	20.340	20.336			
−1	1	1	1L	20.406	20.425	1L	20.774	20.790	1L	20.819	20.817
1	1	3	3	21.572	21.577	4	21.846	21.856	5	21.861	21.864
1	−1	2	6	22.117	22.117	10	22.419	22.427	10	22.483	22.482
−1	−1	3				1	22.959	22.996	1L	23.048	23.085
1	0	4	3	23.267	23.270	3	23.569	23.573	3	23.646	23.631
0	1	4			23.265	2	23.662	23.668	1	23.695	23.675
0	−1	4	1	23.959	23.944	10	24.193	24.222	3	24.313	24.306
−1	0	4	1	24.086	24.078	2	24.441	24.445	1	24.511	24.529
0	0	5	100	24.793	24.787	100	25.145	25.148	86	25.221	25.218
−1	1	3	6	24.869	24.848	16	25.307	25.312	16	25.344	25.346

h	k	l	$AgMn_3Ga(MoO_4)_5$			$AgZn_3Ga(MoO_4)_5$			$AgCo_3Ga(MoO_4)_5$		
			I/I_0	$2\theta_{obs.}$,°	$2\theta_{cal.}$,°	I/I_0	$2\theta_{obs.}$,°	$2\theta_{cal.}$,°	I/I_0	$2\theta_{obs.}$,°	$2\theta_{cal.}$,°
1	1	4	3	25.122	25.119	5	25.459	25.465	6	25.480	25.478
0	2	0	3	25.701	25.697	2	26.072	26.058	2	26.055	26.054
2	0	0	73	25.959	29.954	83	26.307	26.302	100	26.396	26.392
0	2	1	23	26.036	26.025	38	26.417	26.422			26.403
2	0	1	10	26.255	26.250	20	26.596	26.590	18	26.679	26.676
0	−2	1	6	26.337	26.333	22	26.664	26.674	7	26.697	26.690
−1	−1	4	4	26.483	26.488	7	26.780	26.782	7	26.888	26.890
1	2	0	8	26.613	26.601	3	26.883	26.881			26.892
−2	0	1			26.614	7	26.984	26.984	7	27.079	27.081
1	2	1	11	26.835	26.829	25	27.132	27.137	18	27.133	27.131
2	1	1	2	27.007	27.001	5	27.283	27.278	3	27.350	27.345
−1	−2	1	11	27.307	27.306	26	27.575	27.575	19	27.613	27.609
0	2	2			27.285	4	27.712	27.731	3	27.705	27.703
−2	−1	1	3	27.507	27.503	4	27.790	27.784	3	27.880	27.879
0	1	5	6	27.622	27.611	10	28.081	28.084	8	28.109	28.105
0	−2	2	3	27.874	27.873	6	28.208	28.210	5	28.255	28.250
1	2	2	2	27.961	27.970	4	28.320	28.322	4	28.308	28.304
1	−1	4	2	28.066	28.064	6	28.423	28.425	5	28.512	28.510
2	1	2	2	28.114	28.121			28.423	3	28.454	28.481
−2	0	2	2	28.164	28.167	1	28.567	28.573	2	28.672	28.678
0	−1	5	6	28.342	28.336	16	28.678	28.676	13	28.782	28.778
−1	0	5				1	28.893	28.900	1	29.000	28.997
−1	−2	2	1	28.877	28.882	2	29.163	29.159	1	29.223	29.217
−2	−1	2	4	29.081	29.082	10	29.391	29.390	9	29.499	29.501
0	2	3	3	29.376	29.367	4	29.859	29.869	3	29.837	29.839
2	0	3	1L	29.525	29.516	2	29.898	29.888	1	29.985	29.973
0	0	6	1	29.860	29.850	1	30.300	30.287	1	30.383	30.372
1	2	3	1L	29.929	29.927	1	30.365	30.334	1	30.324	30.310
2	1	3	4	30.055	30.056	9	30.397	30.397	9	30.453	30.450
0	−2	3	1L	30.175	30.189	1	30.527	30.539	1	30.590	30.603
−2	0	3	1L	30.513	30.488	1	30.983	30.940	1L	31.055	31.055
−1	−1	5	1L	30.622	30.621			30.981	1	31.088	31.106
−1	2	0	1	30.953	30.949	2	31.460	31.462	1	31.483	31.484
−1	−2	3	2	31.213	31.207	4	31.501	31.509	4	31.594	31.592
−2	1	0				1	31.618	31.616	1L	31.691	31.698
−2	−1	3				2	31.748	31.755	18	31.865	31.883
−1	2	1	8	31.303	31.304	22	31.849	31.854			31.865

Continuation of table 1

h	k	l	$AgMn_3Ga(MoO_4)_5$			$AgZn_3Ga(MoO_4)_5$			$AgCo_3Ga(MoO_4)_5$		
			I/I_0	$2\theta_{obs.}$,°	$2\theta_{cal.}$,°	I/I_0	$2\theta_{obs.}$,°	$2\theta_{cal.}$,°	I/I_0	$2\theta_{obs.}$,°	$2\theta_{cal.}$,°
1	−2	1	2	31.408	31.410	2	31.912	31.899	3	31.945	31.935
2	−1	1	1	31.440	31.428			31.914	1	31.996	31.999
1	−1	5	1	31.853	31.857	3	32.264	32.264	2	32.362	32.364
−1	1	5	1L	31.974	31.980				1	32.590	32.619
0	2	4	2	32.137	32.125	9	32.653	32.689	2	32.654	32.663
2	0	4	4	32.239	32.238			32.647	6	32.741	32.736
2	−1	2	1	32.512	32.535	11	33.027	33.015	1	33.127	33.106
1	2	4	3	32.569	32.567			33.038	7	33.020	33.014
1	−2	2	3	32.655	32.656	5	33.131	33.133	4	33.188	33.186
0	−1	6				2	33.363	33.368			
0	−2	4	7	33.135	33.134	16	33.511	33.513	11	33.603	33.601
2	2	0	1	33.214	33.200			33.510	1	33.551	33.568
2	2	1	2	33.311	33.313	6	33.634	33.641	5	33.683	33.681
−2	0	4	1	33.426	33.434	4	33.935	33.941	1	34.059	34.066
1	1	6	1L	33.460	33.454			33.948			
−2	−2	1	3	33.847	33.852	11	34.158	34.160	8	34.239	34.239

Cu *K*α1 radiation (*l* = 1.54056 Å)

Table 2

Unit-cell parameters for $AgA_3Ga(MoO_4)_5$ (*A* = Mn, Zn, Co)

A	*a*, Å	*b*, Å	*c*, Å	α°	β°	γ°	*V*, Å^3
Mn	6.9844 (3)	7.0519 (4)	17.9700 (8)	87.796 (4)	87.529 (5)	79.386 (4)	868.71
Zn	6.9037 (3)	6.9639 (4)	17.7147 (8)	88.107 (4)	87.440 (4)	78.982 (4)	834.87
Co	6.8810 (4)	6.9657 (4)	17.669 (1)	87.895 (5)	87.344 (5)	78.976 (5)	830.04

atomic coordinates, isotropic atomic displacement parameters, cation occupancies and main selected interatomic distances are presented in Tables 4 and 5. The populations of four independent positions *M* = (Zn, Ga) and three incompletely occupied Ag sites were refined with keeping the electrical neutrality of the chemical formula. The final compositions of the crystals are close to stoichiometric $AgZn_3Ga(MoO_4)_5$ with a negligible silver deficiency.

In the structure $AgZn_3Ga(MoO_4)_5$ all atoms are located in general positions. Coordination polyhedra of Mo atoms are tetrahedra with Mo–O distances of 1.714–1.824 Å, which are similar to the values found in other molybdates containing a tetrahedral anion. Cations Zn^{2+} and Ga^{3+} are statistically distributed on octahedral positions *M*1–*M*4 with the (Zn, Ga)–O bond lengths of 1.940–2.129 Å. Both Ag1 and Ag3 cations are coordinated by four O atoms (Ag1–O 2.358 Å, Ag3–O 2.415 Å), while Ag2 cation has CN = 5 (Ag2–O 2.495 Å). The structure of $AgZn_3Ga(MoO_4)_5$ consists of MoO_4 tetrahedra, couples of edge-shared $M(1)O_6$ octahedra, and trimers of edge-shared $M(2)O_6$, $M(3)O_6$ and

Table 3

Crystal data and structure refinement for $AgZn_3Ga(MoO_4)_5$

Structural formula	$AgZn_3Ga\ (MoO_4)_5$
Formula weight, M_r (g mol^{-1})	1172.58
Temperature (K)	298(2)
Crystal system, space group (#)	Triclinic, $P\bar{1}$ (2)
Unit-cell parameters:	
a (Å)	6.9035 (5)
b (Å)	6.9643 (5)
c (Å)	17.7160 (14)
α (°)	88.1039 (11)
β (°)	87.4338 (12)
γ (°)	78.9880 (9)
Unit-cell volume, V (Å^3)	835.0 (2)
Formula unit, Z	2
Calculated density, ρ_{cal} (g cm^{-3})	4.66
Refinement R factors and goodness of fit:	
wR_p	0.0511
R_p	0.0382
R_{exp}	0.0152
$R(F^2)$	0.05815
χ^2	3.40

Table 4

Structural parameters for $AgZn_3Ga(MoO_4)_5$

Atom	**Occupancy**	***x***	***y***	***z***	***Uiso***
Mo1	1	0.2722(8)	0.3095(8)	0.5282(3)	0.030(2)
Mo2	1	0.2129(8)	0.8293(9)	0.2856(3)	0.028(2)
Mo3	1	0.6843(8)	0.2187(8)	0.3109(3)	0.023(2)
Mo4	1	0.2811(9)	0.0522(9)	0.9044(3)	0.029(2)
Mo5	1	0.2520(8)	0.5491(8)	0.0863(3)	0.021(2)
*M*1	0.788(1)Zn+0.212(1)Ga	0.1834(12)	0.8241(11)	0.4938(5)	0.0126(3)
*M*2	0.901(1)Zn+0.099(1)Ga	0.1704(14)	0.0855(16)	0.1145(5)	0.045(4)
*M*3	0.798(1)Zn+0.202(1)Ga	0.7829(12)	0.4310(13)	0.1239(4)	0.014(3)
*M*4	0.505(1)Zn+0.495(1)Ga	0.2546(12)	0.3014(13)	0.7370(4)	0.023(3)
Ag1	0.323(3)Ag	0.149(3)	0.339(3)	0.2857(12)	0.062(5)
Ag2	0.328(3)Ag	0.122(4)	0.308(4)	0.3155(13)	0.062(5)
Ag3	0.342(3)Ag	0.097(3)	0.370(3)	0.3445(11)	0.062(5)
O1	1	0.511(5)	0.194(5)	0.5163(18)	0.015(1)
O2	1	0.289(4)	0.366(4)	0.6238(17)	0.015(1)
O3	1	0.171(4)	0.545(5)	0.4601(18)	0.015(1)
O4	1	0.130(5)	0.126(5)	0.4978(18)	0.015(1)

Continuation of table 4

Atom	Occupancy	*x*	*y*	*z*	*Uiso*
O5	1	0.189(4)	0.872(4)	0.3866(18)	0.015(1)
O6	1	0.477(5)	0.719(4)	0.2580(17)	0.015(1)
O7	1	0.140(5)	0.053(5)	0.2220(19)	0.015(1)
O8	1	0.098(5)	0.641(5)	0.2687(18)	0.015(1)
O9	1	0.419(5)	0.280(4)	0.3590(17)	0.015(1)
O10	1	0.804(5)	0.191(4)	0.3830(18)	0.015(1)
O11	1	0.681(5)	0.995(5)	0.2696(17)	0.015(1)
O12	1	0.774(4)	0.370(5)	0.237(2)	0.015(1)
O13	1	0.198(4)	0.121(4)	0.997(2)	0.015(1)
O14	1	0.468(5)	0.040(4)	0.0841(15)	0.015(1)
O15	1	0.831(5)	0.202(5)	0.1174(16)	0.015(1)
O16	1	0.238(4)	0.305(5)	0.8544(17)	0.015(1)
O17	1	0.249(4)	0.546(4)	0.987(2)	0.015(1)
O18	1	0.485(5)	0.488(5)	0.1153(17)	0.015(1)
O19	1	0.171(4)	0.778(5)	0.1292(18)	0.015(1)
O20	1	0.097(4)	0.410(5)	0.1173(18)	0.015(1)

$M(4)O_6$ octahedra, which are linked by the common vertices to form a 3D framework (Fig. 2). In the large framework cavities, the silver cations are disordered on three close positions with the distances Ag–Ag 0.595(4) Å and 1.101(2) Å.

Such a disordering is also typical of other compounds of this isostructural series [7, 9], suggesting a possible mobility of the Ag^+ cations in the compounds. This is favored not only by defects in Ag positions along with their irregular coordina-

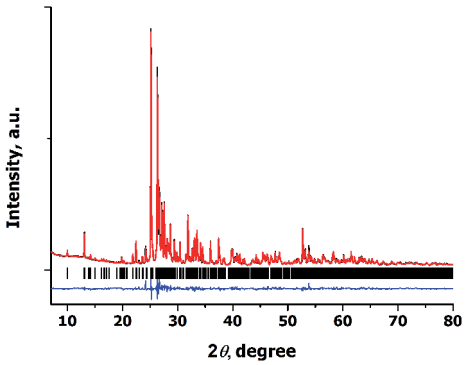

Fig. 1. Observed (black line) and calculated (red line) XRD patterns of $AgZn_3Ga(MoO_4)_5$. Vertical bars indicate the positions of the Bragg peaks. The lower trace depicts the difference between the experimental and calculated intensity values

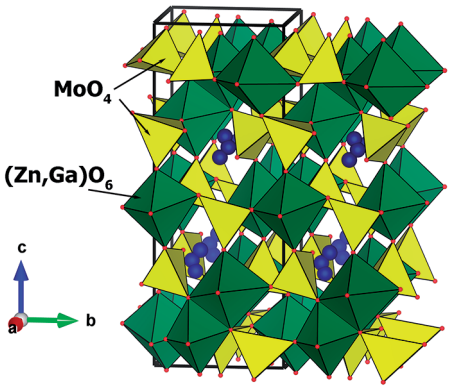

Fig. 2. Projection views of the structure of $AgZn_3Ga(MoO_4)_5$ along the *a* axis. The blue spheres and small red spheres indicate Ag and oxygen atoms, respectively

Table 5

Selected interatomic distances(Å) in $AgZn_3Ga(MoO_4)_5$

Mo1-tetrahedron		**Mo2-tetrahedron**	
Mo1–O1	1.696(3)	Mo2–O5	1.819(3)
–O2	1.764(3)	–O6	1.889(3)
–O3	1.726(3)	–O7	1.891(3)
–O4	1.858(3)	–O8	1.698(3)
<Mo1–O>	1.761	<Mo2–O>	1.824
Mo^3-tetrahedron		**Mo4-tetrahedron**	
Mo3–O9	1.961(3)	Mo4–O13	1.749(3)
–O10	1.739(3)	–O14	1.726(2)
–O11	1.747(4)	–O15	1.922(3)
–O12	1.812(3)	–O16	1.760(3)
<Mo3–O>	1.815	<Mo4–O>	1.789
Mo5-tetrahedron		***M*1-octahedron**	
Mo5–O17	1.758(4)	*M*1–O1	2.092(3)
–O18	1.683(3)	–O3	2.068(3)
–O19	1.773(3)	–O10	2.186(3)
–O20	1.640(3)	–O4	2.070(2)
<Mo5–O>	1.714	–O5	1.918(3)
		–O4	2.124(3)
		<*M*1–O>	2.076
***M*2-octahedron**		***M*3-octahedron**	
*M*2–O7	1.918(3)	*M*3–O18	2.030(3)
–O13	2.096(3)	–O17	1.99(4)
–O19	2.144(3)	–O15	1.572(3)
–O20	2.224(3)	–O16	1.869(3)
–O14	2.066(3)	–O12	2.038(3)
–O15	2.325(3)	–O20	2.143(3)
<*M*2–O>	2.129	<*M*3–O>	1.940
***M*4-octahedron**		**Ag1-polyhedron**	
*M*4–O8	2.398(4)	Ag1–O9	2.29(4)
–O11	2.033(4)	–O8	2.080(3)
–O2	2.053(3)	–O7	2.33(4)
–O6	1.837(3)	–O12	2.73(4)
–O16	2.079(3)	<Ag1–O>	2.358
–O12	2.320(3)		
<*M*4–O>	2.120		
Ag2-polyhedron		**Ag3-polyhedron**	
Ag2–O9	2.19(4)	Ag3–O9	2.22(4)
–O10	2.70(4)	–O8	2.28(4)
–O8	2.41(4)	–O10	2.62(4)
–O7	2.45(4)	–O3	2.540(3)
–O12	2.725(3)	<Ag3–O>	2.415
<Ag2–O>	2.495		
Ag1–Ag2	0.595(4)		
Ag1–Ag3	1.101(2)		

tion, but also a rather flexible polyhedral framework of the $NaMg_3In(MoO_4)_5$ structure type, which involves interconnected cavities.

Electrophysical properties

As was noted in the previous section, the structural features of the obtained molybdates allow us to expect these compounds to have the increased ionic conductivity. This was already confirmed by us in the case of $AgMg_3Al(MoO_4)_5$ ($\sigma = 2.5 \times 10^{-2}$ S/cm) and $AgMn_3Al(MoO_4)_5$ ($\sigma = 7.1 \times 10^{-3}$ S/cm) at 500 °C [7]. In this work as an example, the results of studying electrophysical properties for $AgMn_3Ga(MoO_4)_5$ are presented.

It was found that the DC conductivity of ceramic sample $AgMn_3Ga(MoO_4)_5$, measured with the V7–38 device, is negligible as compared to the ac conductivity (Fig. 3) in temperature region of 100–560 °C. As the platinum electrodes are blocking in the DC conductivity measurement mode, the DC conductivity of $AgMn_3Ga(MoO_4)_5$ corresponds to the electronic one. Therefore, it can be concluded that the AC conductivity is almost equal to the ionic one.

It is seen that near room temperature the conductivity is as small as 10^{-7} S/cm

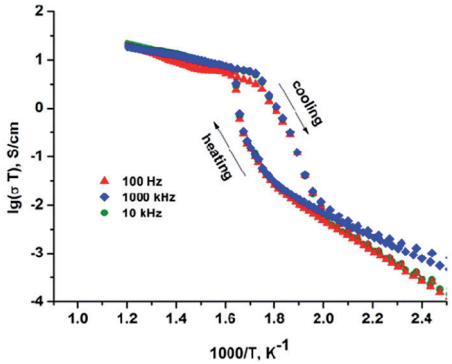

Fig. 3. Temperature dependences of the ionic conductivity on heating and cooling for $AgMn_3Ga(MoO_4)_5$

but quickly rises with temperature to values of about 10^{-2} S/cm. It is noteworthy that the conductivity in $AgMn_3Ga(MoO_4)_5$ increases with temperature in non-monotonic way showing distinct breaks on $\lg\sigma = f(1/T)$ curves at 310 °C. Above these temperature the $\lg\sigma = f(1/T)$ dependences are almost linear with the small activation energy value $E_a = 0.26$ eV. Above 310 °C, the ionic conductivity of $AgMn_3Ga(MoO_4)_5$ increases up to $2.03 \cdot 10^{-2}$ S/cm at 500 °C, which is close to the corresponding characteristics of the known ionic conductors.

Conclusions

The possibility of the formation of silver-containing gallium triple molybdates with Mn, Co, Zn, Ni, analogous to the phases $Ag_{1-x}A_{1-x}R_{1+x}(MoO_4)_3$ and $AgA_3R(MoO_4)_5$ obtained by us in the Ag_2MoO_4–$AMoO_4$–$R_2(MoO_4)_3$ (A = Mg, Co; R = Al; A = Mg, R = In) systems, was studied. It was shown that in the Ag_2MoO_4–$AMoO_4$–$Ga_2(MoO_4)_3$ (A = Mn, Co, Zn, Ni) systems the NASICON-like phases of the composition $Ag_{1-x}A_{1-x}R_{1+x}(MoO_4)_3$ are not formed. The triple molybdates of the composition $AgA_3Ga(MoO_4)_5$ (A = Mn, Co, Zn) were synthesized and characterized. $AgNi_3Ga(MoO_4)_5$ was not obtained in the single-phase state. It was established that the obtained compounds incongruently melt and belong to the structural type of triclinic $NaMg_3In(MoO_4)_5$ (sp. gr. $P\bar{1}$, Z = 2). The structure of the obtained compounds was refined by the Rietveld method using the powder diffraction data for $AgZn_3Ga(MoO_4)_5$. The structural features of the obtained molybdates allow us to expect these compounds to have the increased ionic conductivity. This was

confirmed by studying electrophysical properties of $AgMn_3Ga(MoO_4)_5$. It was shown that the high-temperature electrical conductivity of this compound reaches 10^{-2} S/cm at E_a = 0.26 eV, which is close to the corresponding characteristics of the known ionic conductors.

Acknowledgments

The research was carried out within the state assignment of BINM SB RAS, supported in part by the Russian Foundation for Basic Research (Project No. 17-03-00333a)

References

1. Kotova IYu. Phase formation in the Ag_2MoO_4–$CoMoO_4$–$Al_2(MoO_4)_3$ system. *Russ J Inorg Chem*. 2014;59:844–8. DOI:10.7868/S0044457X14080133.
2. Kotova IYu, Korsun VP. Phase in the Ag_2MoO_4–$MgMoO_4$–$Al_2(MoO_4)_3$. *Russ J Inorg Chem*. 2010;55:955–8. DOI: 10.1134/S0036023610060203.
3. Kotova IYu, Korsun VP. Phase formation in the system involving silver, magnesium, and indium molybdates. *Russ J Inorg Chem*. 2010;55:1965–9. DOI: 10.1134/S0036023610120247.
4. Kotova IYu, Belov DA, Stefanovich SYu. $Ag_{1-x}Mg_{1-x}R_{1+x}(MoO_4)_3$ Ag^+-conducting NASICON-like phases, where R = Al or Sc and $0 \le x \le 0.5$. *Russ J Inorg Chem*. 2011;56:1189–93. DOI: 10.1134/S0036023611080122.
5. Bouzidi C, Frigui W, Zid MF. Synthèse et structure crystalline d'un matériau noir $AgMn^{II}_3(Mn^{III}_{0.26}Al_{0.74})(MoO_4)_5$. *Acta Cryst*. 2015; E71:299–304. DOI: 10.1107/S2056989015003345.
6. Nasri R, Chérif SF, Zid MF. Structure cristalline de la triple molybdate $Ag_{0.90}Al_{1.06}Co_{2.94}(MoO_4)_5$. *Acta Cryst*. 2015; E71:388–91. DOI: 10.1107/s2056989015005290.
7. Kotova IYu, Solodovnikov SF, Solodovnikova ZA, Belov DA, Stefanovich SYu, Savina AA, Khaikina EG. New series of triple molybdates $AgA_3R(MoO_4)_5$ (A = Mg, R = Cr, Fe; A = Mn, R = Al, Cr, Fe, Sc, In) with framework structures and mobile silver ion sublattices. *J Solid State Chem*. 2016;238:121–8. DOI: 10.1016/j. jssc. 2016.03.003.
8. Balsanova LV. Synthesis of crystals of silver containing oxide phases based on molybdenum, study of their structure and properties. *Vestnik VSGUTU*. 2015;5:63–9.
9. Kotova IYu, Savina AA, Khaikina EG. Crystal structure of new triple molybdate $AgMg_3Ga(MoO_4)_5$ from Rietveld refinement. *Powder Diffraction*. 2017;32(4):255–60. DOI: 10.1017/S0885715617000811.
10. Yanushkevich TM, Zhukovsky VM, Ustyantsev VM. Fazovaya diagramma sistemy NiO-MoO_3. [Phase diagram of the system NiO-MoO_3]. *Russ J Inorg Chem*. 1974;19(7):1932–6.
11. Zhukovsky VM, Tkachenko EV. Fazovye ravnovesiya v molibdatnykh sistemakh. [Phase equilibria in molybdate systems]. Zbornik nauchnykh trudov. *"Fizicheskaya khimiya okislov"*. Moscow: Nauka; 1981.106–15. Russian.
12. Reichelt W, Weber T, Soehnel T. at al. Electronic structure and luminescence mechanisms in $ZnMoO_4$ crystals. *J Phys: Condes Mater*. 2011;23:244-59.
13. Tsyrenova GD, Bazarova JG, Mokhosoev MV. Phase equilibria in systems MeO–MoO_3 (Me–Mg, Mп, Zn). *Russ J Inorg Chem*. 1986;31(12):3120–3.

14. Rajaram P, Viswanathan B, Aravamudan G. Studies on the formation of manganese molybdates. *Thermochim acta*. 1973;7 (2):123–9.
15. Kohlmuller R, Faurie J.-P. Etude des systemes MoO_3–Ag_2MoO_4 et MoO_3–MO (M–Cu, Zn, Cd). *Bull Soc chim. France*. 1968;11:4379–82.
16. Larson AC, Von Dreele RB. General Structure Analysis System (GSAS) (Report LAUR 86–748). 2004. Los Alamos, New Mexico: Los Alamos National Laboratory.
17. Shannon RD. Revised effective ionic radii and systematic studies of interatomic distances in dalides and chalcogenides. *Acta Cryst*. 1976; A32:751–67. DOI: 10.1107/S0567739476001551.
18. Gates Stacy D, Julie A, Lind C. Gates Non-hydrolytic sol-gel synthesis, properties, and high-pressure behavior of gallium molybdate. *J Mater Chem*. 2006;16:4214–9. DOI:10.1039/B608864C.
19. Perepelitsa AP, Golub AM, Badayev YuB, Shapoval VN. Double molybdates of aluminum, gallium, indium, chromium, iron and bismuth with monovalent silver and thallium. *Russ J Inorg Chem*. 1977;22(4):994–7.
20. Klevtsova RF, Vasiliev AD, Kozhevnikova NM, Glinskaya LA, Kruglik AI, Kotova IYu. Synthesis and crystal structural study of ternary molybdate $NaMg_3In(MoO_4)_5$. *J Struct Chem*. 1994;34:784–8.
21. Rietveld HM. A profile refinement method for nuclear and magnetic structures. *J Appl Cryst*. 1969;2:65–71.

Cijin J. George, Sougata Santra, Zyryanov G. V., Kousik Giri
Chimica Techno Acta. 2018. Vol. 5, No. 3. P. 144–149.
ISSN 2409–5613

DOI: 10.15826/chimtech.2018.5.03.03

Cijin J. George[1], Sougata Santra[2], G. V. Zyryanov[2,3], Kousik Giri[1*]

[1]*Department of Computational Sciences, Central University of Punjab, Bathinda, Punjab, India*
[2]*Department of Organic and Biomolecular Chemistry, Chemical Engineering Institute, Ural Federal University, 19 Mira St., Ekaterinburg, 620002, Russian Federation*
[3]*I. Ya. Postovskiy Institute of Organic Synthesis, Ural Branch of the Russian Academy of Sciences, 22 S. Kovalevskoy St., Ekaterinburg, 620219, Russian Federation*
**E-mail: kousikgiri@gmail.com*

Arsenate and Arsenite Reaction Kinetics with Ferric Hydroxides Using Quantum Chemical Calculations

The knowledge of the mechanism involved in the process of adsorption and desorption of arsenate and arsenite with ferric hydroxides is important to address the water toxicity problems and to tackle the adverse effect of these substances in nature. An essential outcome of previous studies on the kinetics of the arsenate adsorption on aluminum and iron oxide was that the adsorption is a two-phase (bi-phase) process. Quantum mechanical calculations using density functional theory were used to determine the thermodynamic variables governing the adsorption process to get an insight into the stability of the complexes formed. The previous investigation showed that the positively charged ferric hydroxide cluster had better stability at neutral pH. The chemisorbed charged monodentate complexes had Gibbs free energy of reaction –55.97 kcal/mol where the bidentate complex formation had Gibbs free energy of reaction –62.55 kcal/mol. The bidentate complex having a negative charge had more Gibbs free energy of reaction compared to uncharged one. The results of the study indicate that Gibbs free energy for the reaction has a significant role in controlling the kinetics of the adsorption and sorption process of arsenate on ferric hydroxide clusters.

Keywords:

Received: 01.10.2018. Accepted: 25.10.2018. Published: 31.10.2018.

Introduction

Arsenic is a significant contaminant present in the groundwater due to natural processes like weathering of rocks, discharge of effluents and waste disposal from industries, arsenical herbicides and pesticides used in agricultural activities and many other sources [1]. The various oxidation states arsenic exhibits are –3, 0, +3, and +5, where the inorganic forms +3 (arsenite) and +5 (arsenate) states of As are

predominant depending on the reducing and oxidizing conditions, respectively. The relatively strong adsorption affinity of As shown towards ferric hydroxides has a vital role in the detoxification of As, thereby controlling the arsenic water pollution and employed in techniques for purification of drinking water.

Several works were done on the structural determination of arsenate-ferric hydroxide complex. The studies of arsenic (III) stability on goethite using X-ray absorption spectroscopy and batch techniques indicated that there is inner sphere bidentate complexation through ligand exchange [2]. Monodentate and bidentate complexes are observed in the adsorption of arsenate on goethite [3–5]. The models produced by molecular modeling and the X-ray absorption fine structure spectroscopy (EXAFS) results are compared, and the nature of the chemisorption complex is determined [6, 7]. An essential outcome of previous studies on the kinetics of the arsenate adsorption on aluminum and iron oxide was the two-phase adsorption process constituting a fast phase of the time order of a minute or less and slow phase which attains an equilibrium within a time scale greater than 162 hours [5, 8–10]. The factors responsible for this phenomenon are considered to be slow diffusion mass transport [9, 11, 12], availability of heterogeneous sites, monodentate to bidentate complex conversions, the surface precipitate formation and the rearrangement of surface complexes. Further, the studies on the arsenate desorption by use of different extractants like phosphate or high pH solutions indicate a slow release of arsenate from the adsorbed complexes. The conclusion from these studies implies that only a small portion of arsenate is released by the use of extractants like phosphate or hydroxide ions. This leads to the interesting fact that a part of arsenate-ferric hydroxide complex may be irreversible in nature.

Despite the studies done on arsenate-ferric hydroxide complex formation, a little is known about the mechanism of this reaction. In this regard, the motive of this theoretical study is to get an insight into the mechanism governing the arsenate-ferric hydroxide complex formation. The thermodynamic parameters and reaction rates governing the mechanism are determined by quantum chemical calculations.

Materials and Methods

All calculations were carried out using the Gaussian 09 software [13]. Full geometry optimizations and corresponding harmonic vibrational frequency computations, to confirm their minima on the potential energy surface, were carried out using the Austin-Frisch-Petersson functional with dispersion (APFD) [14] and M06 hybrid functional of Truhlar and Zhao [15] suite of density functional theories (DFT) as implemented in Gaussian 09. APFD functional has been used as a primary method in Gaussian 09 for its best trade-off between accuracy and computational cost for the largest range of molecular systems and chemical problems. M06 functional perform better for a model system with dispersion and ionic hydrogen-bonding interactions. For both structural optimizations and frequency calculations the balanced basis set of triple zeta valence from Ahlrichs and coworkers (DEF2TZVP) [16] was employed. For all calculations, solvent effects of water were introduced using the polarizable continuum model (PCM) using the integral equation formalism variant

(IEFPCM) with APFD functional and the SMD variation of IEFPCM of Truhlar and workers with M06 functional.

Quantum-chemical calculations involving DFT were used to calculate the heat of formation of reactants and products and their corresponding Gibbs free energies. The ferric hydroxides clusters were modeled following the previous studies. The ferric hydroxides clusters consisted of two iron atoms, ten oxygen atoms which were octahedrally coordinated to the iron atoms. The clusters can be represented by the general formula $Fe_2O_3\ (H_2O)_7$. The numbers of the protons were varied to calculate the effect of binding of arsenate with the cation and anion cluster's binding sites.

To minimize the effect of gross distortions of the di-octahedral geometry observed in previous studies [17], the coordinates of six peripheral oxygen atoms which were not part of the binding reaction was fixed to simulate the binding sites of the iron hydroxide clusters also including bound arsenic species. The enthalpies of the reaction are determined by calculating the heats of formation. The equation used is as follows:

$$\Delta_r H_0(298\text{K}) = \\ = \Sigma(E_0 + H_{\text{corr}})_{\text{products}} - (E_0 + H_{\text{corr}})_{\text{reactants}}$$

Similarly, Gibbs free energy change of the reaction is computed by the key equation:

$$\Delta_r G_0(298\text{K}) = \\ = \Sigma(E_0 + G_{\text{corr}})_{\text{products}} - (E_0 + G_{\text{corr}})_{\text{reactants}}$$

Results and Discussion

The heat of formation of the clusters at 0K was determined and is given in Table 1.

Table 1

Calculated heat of formation for three different possible species

Cluster	Charge	Heat of Formation (kcal/mol)
$Fe_2O_{10}H_{13}^-$	–1	–1261.64
$Fe_2O_{10}H_{14}$	0	–1186.33
$Fe_2O_{10}H_{15}^+$	+1	–1087.94

The results indicate that the heat of formation of the positive charged ferric hydroxide has the least value at 0K, whereas the other clusters are more stable than $Fe_2O_{10}H_{15}^+$. The previous investigation showed that the positively charged ferric hydroxide cluster had better stability at neutral pH [17]. This may be possible due to the better stabilization of the $Fe_2O_{10}H_{15}^+$ at neutral pH and hence increase in the heat of formation at the neutral pH. The optimized geometry of the $Fe_2O_{10}H_{15}^+$ is represented by Fig. 1.

The reaction of $Fe_2O_{10}H_{15}^+$ with $HAsO_4^{2-}$ resulted in the formation of charged (–1 charge) monodentate (Fig. 2) and bidentate complex (Fig. 3).

Meanwhile, the reaction of $Fe_2O_{10}H_{15}^+$ with $H_2AsO_4^-$ resulted in the formation of uncharged monodentate (Fig. 4) and bidentate complex (Fig. 5).

The corresponding Gibbs free energy for the reaction was determined for the monodentate and bidentate complexes formed. The values are in given in table two and three, respectively.

The mono- and bidentate complex bearing a negative charge showed higher stability than the uncharged complexes formed. This indicates that the charge on the species improved the stability of the complex. The chemisorbed charged monodentate complexes had Gibbs free energy of reaction –55.97 kcal/mol, whereas the bidentate complex formation had Gibbs free energy of reaction –62.55 kcal/mol. Thus, the desorption process of arsenate with com-

petitive ligands would depend on Gibbs free energy of the reaction. The process is feasible only when the higher Gibbs free energy values are attained. The results of the study indicate that Gibbs free energy for the reaction has a significant role in controlling the kinetics of the adsorption and sorption process of arsenate on ferric hydroxide clusters.

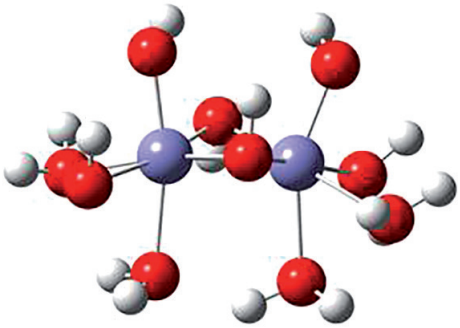

Fig. 1. Structure of $Fe_2O_{10}H_{15}^+$ complex carrying a net positive charge

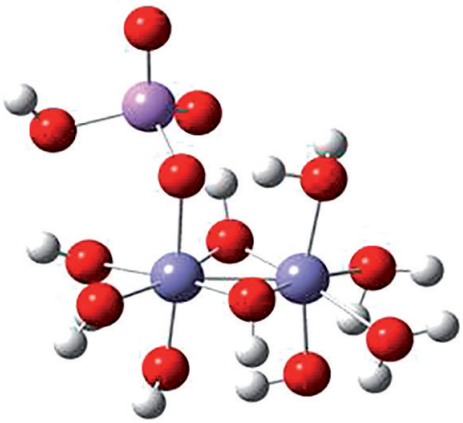

Fig. 2. Structure of negatively charged monodentate complex

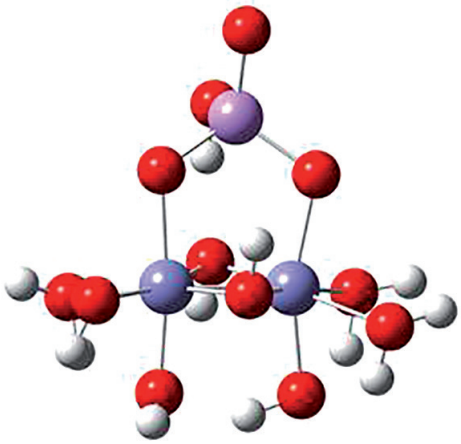

Fig. 3. Structure of negatively charged bidentate complex

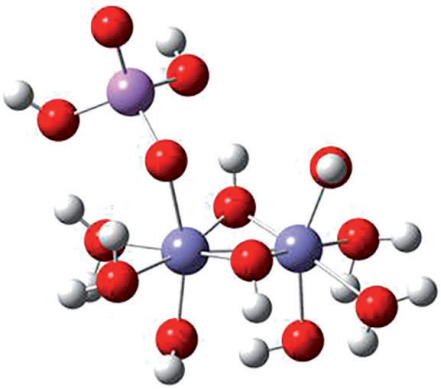

Fig. 4. Structure of uncharged monodentate complex

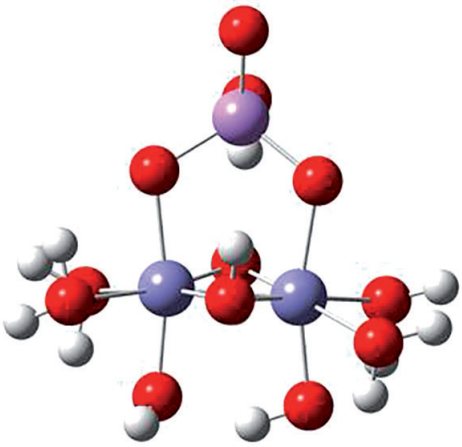

Fig. 5. Structure of uncharged bidentate complex

Table 2

Thermochemical analysis of negatively charged monodentate and bidentate complexes

Method	Product I–Mono Dentate			Product-II Bidentate		
	$\Delta_r E$ (kcal/mol)	$\Delta_r H$ (kcal/mol)	$\Delta_r G$ (kcal/mol)	$\Delta_r E$ (kcal/mol)	$\Delta_r H$ (kcal/mol)	$\Delta_r G$ (kcal/mol)
APFD	–61.3202283	–106.9803296	–55.9700823	–57.8908889	–57.0832842	–62.5564221
M06				–30.9876741	–30.0162894	–36.3949235

Table 3

Thermochemical analysis of uncharged monodentate and bidentate complexes

Method	Product I–Mono Dentate			Product-II Bidentate		
	$\Delta_r E^0$ (kcal/mol)	$\Delta_r H$ (kcal/mol)	$\Delta_r G$ (kcal/mol)	$\Delta_r E$ (kcal/mol)	$\Delta_r H$ (kcal/mol)	$\Delta_r G$ (kcal/mol)
APFD	–32.0525578	–31.7544907	–28.0741475	–38.3383204	–37.5514235	–43.1638684
M06	–16.7174805	–15.8289271	–13.6307614	–20.3865286	–18.4719972	–27.6141831

Acknowledgments

K. Giri acknowledges financial support from UGC, Govt. of India for Start-up Project Funding. S. Santra and G. V. Zyryanov thank Russian Science Foundation (Ref # 18-73-00301) for financial help.

References

1. Bhumbla DK, Keefer RF. Arsenic mobilization and bioavailability in soils. *Arsenic in the Environment*. Part I: Cycling and Characterization. Nriagu JO, Editor. John Wiley & Sons: New York, 1994. pp 51–82.
2. Manning BA, Fendorf SE, Goldberg S. Surface Structures and Stability of Arsenic (III) on Goethite: Spectroscopic Evidence for Inner-Sphere Complexes. *Environmental Science & Technology*. 1998;32(16):2383–8. DOI: 10.1021/es9802201.
3. Waychunas GA, Davis JA, Fuller CC. Geometry of sorbed arsenate on ferrihydrite and crystalline FeOOH: Re-evaluation of EXAFS results and topological factors in predicting sorbate geometry, and evidence for monodentate complexes. *Geochimica et Cosmochimica Acta*. 1995;59 (17):3655–61. DOI: 10.1016/0016–7037(95) 00276–6.
4. Waychunas GA, Rea BA, Fuller CC, Davis JA. Surface chemistry of ferrihydrite: Part 1. EXAFS studies of the geometry of coprecipitated and adsorbed arsenate. *Geochimica et Cosmochimica Acta*. 1993;57(10):2251–69. DOI: 10.1016/0016–7037(93)90567-G.
5. Grossl PR, Eick M, Sparks DL, Goldberg S, Ainsworth CC. Arsenate and Chromate Retention Mechanisms on Goethite. 2. Kinetic Evaluation Using a Pressure-Jump Relaxation Technique. *Environmental Science & Technology*. 1997;31(2):321–6. DOI: 10.1021/es950654l.
6. Kubicki JD. Comparison of As (III) and As (V) Complexation onto Al- and Fe-Hydroxides. Advances in Arsenic Research. *ACS Symposium Series*. 915: American Chemical Society; 2005. p. 104–17.

7. Sherman DM, Randall SR. Surface complexation of arsenic (V) to iron (III) (hydr) oxides: structural mechanism from ab initio molecular geometries and EXAFS spectroscopy. *Geochimica et Cosmochimica Acta*. 2003;67(22):4223–30. DOI: 10.1016/S0016–7037(03)00237–0.
8. Zhang H, Selim HM. Kinetics of Arsenate Adsorption–Desorption in Soils. *Environmental Science & Technology*. 2005;39(16):6101–8. DOI: 10.1021/es050334u.
9. Fuller CC, Davis JA, Waychunas GA. Surface chemistry of ferrihydrite: Part 2. Kinetics of arsenate adsorption and coprecipitation. *Geochimica et Cosmochimica Acta*. 1993;57(10):2271–82. DOI: 10.1016/0016–7037(93) 90568-H.
10. Yang W, Zhao N, Zhang N, Chen W, Kan AT, Tomson MB. Time-dependent adsorption and resistant desorption of arsenic on magnetite nanoparticles: kinetics and modeling. *Desalination and Water Treatment*. 2012;44(1-3):100–9. DOI: 10.1080/19443994.2012.691808.
11. Raven KP, Jain A, Loeppert RH. Arsenite and Arsenate Adsorption on Ferrihydrite: Kinetics, Equilibrium, and Adsorption Envelopes. *Environmental Science & Technology*. 1998;32 (3):344–9. DOI: 10.1021/es970421p.
12. Luengo C, Brigante M, Avena M. Adsorption kinetics of phosphate and arsenate on goethite. A comparative study. *Journal of Colloid and Interface Science*. 2007;311(2):354–60. DOI: https://doi.org/10.1016/j. jcis. 2007.03.027.
13. Austin A, Petersson GA, Frisch MJ, Dobek FJ, Scalmani G, Throssell K. A Density Functional with Spherical Atom Dispersion Terms. *Journal of Chemical Theory and Computation*. 2012;8(12):4989–5007. DOI: 10.1021/ct300778e.
14. Gaussian09, Revision D. 01, Gaussian, Inc., Wallingford CT, 2013.
15. Zhao Y, Truhlar DG. The M06 suite of density functionals for main group thermochemistry, thermochemical kinetics, noncovalent interactions, excited states, and transition elements: two new functionals and systematic testing of four M06-class functionals and 12 other functionals. *Theoretical Chemistry Accounts*. 2008;120(1):215–41. DOI: 10.1007/s00214-007-0310-x.
16. Weigend F, Ahlrichs R. Balanced basis sets of split valence, triple zeta valence and quadruple zeta valence quality for H to Rn: Design and assessment of accuracy. *Phys Chem Chem Phys*. 2005;7(18):3297–305. DOI: 10.1039/B508541A.
17. Farrell J, Chaudhary BK. Understanding Arsenate Reaction Kinetics with Ferric Hydroxides. *Environmental Science & Technology*. 2013;47(15):8342–7. DOI: 10.1021/es4013382.

Nikonov I. L., Kopchuk D. S., Khasanov A. F., Krinochkin A. P., Starnovskaya E. S., Shtaiz Ya. K., Savchuk M. I, Tanya O. S., Zyryanov G. V., Rusinov V. L., Chupakhin O. N.
Chimica Techno Acta. 2018. Vol. 5, No. 3. P. 150–152.
ISSN 2409–5613

DOI: 10.15826/chimtech.2018.5.3.04

I. L. Nikonov[1,2], D. S. Kopchuk[1,2], A. F. Khasanov[1,2], A. P. Krinochkin[1,2], E. S. Starnovskaya[1], Ya. K. Shtaiz[1], M. I Savchuk[1], O. S. Tanya[1], G. V. Zyryanov[1,2], V. L. Rusinov[1,2], O. N. Chupakhin[1,2]

[1]*Ural Federal University, 19 Mira St., Ekaterinburg 620002, Russian Federation*
[2]*I. Ya. Postovskii Institute of Organic Synthesis, Ural Branch of Russian Academy of Sciences, 22 Kovalevskaya St./20 Akademicheskaya St., Ekaterinburg 620990, Russian Federation*
E-mail: dkopchuk@mail.ru

Two mutually complementary synthetic approaches towards 3-substituted 3,4-disubstituted and 1-(2-pyridyl)-substituted isoquinolines

Two mutually complementary synthetic approaches towards 3- and 3,4-disubstituted 1-(2-pyridyl) isoquinolines were studied. The aryne-based method was successfully used for the obtaining of the corresponding the 3-cyano-1-(2-pyridyl)isoquinolines in one step/pot reaction, while it is unacceptable for the obtaining of other 1-(2-pyridyl)isoquinolines. The enamine-based approach was successfully applied for the synthesis of other 1-(2-pyridyl)isoquinolines, while it was unacceptable for the obtaining of 3-cyano-1-(2-pyridyl)isoquinolines.

Keywords: 1,2,4-triazines; arynes; enamines; isoqunolines; aza-Diels-Alder reaction; domino-transfrormation.

Received: 08.09.2018. Accepted: 19.10.2018. Published: 31.10.2018.

Results and Discussion

Aryne intermediates, generated *in situ*, are currently attracting more and more attention from the point of view of their use in organic synthesis, since practically useful products of various purposes can be obtained [1–3]. Recently, we have demonstrated the possibilities of their successful use in reactions with substituted 1,2,4-triazines for obtaining both the expected aza-Diels-Alder reaction products, namely the corresponding isoquinolines, and the domino transformations, for example, 10-(1*H*- 1,2,3-triazol-1-yl) pyrido [1,2-*a*] indoles. The direction of the reaction depends on the nature of the 1,2,4-triazines (or aryns) introduced into the composition of the substituents [4].

This article analyzes the two synthetic approaches we have developed for the synthesis of 1- (2-pyridyl) isoquinolines with different substituents in the C3 and C4 positions, which are of interest, in particular, as ligands for transition metal cations [5], as well as from the point of view of creating OLED [6].

Thus, the reaction of 3-(2-pyridyl) -1,2,4-triazines **1a**, having an aromatic substituent or a hydrogen atom at the C5 position, with aryne results in the corresponding pyrido [1,2-a] indoles **2** [7] (scheme 1), while the synthesis of target 1-(2-pyridyl) isoquinolines **3a** in this way is impossible. To solve this problem, we developed an alternative synthetic approach, which was based on the use of 3-(2-pyridyl)-1,2,4-triazines **1** as starting compounds. The approach involves the preparation of 5,6,7,8-tetrahydroisoquinolines **4a** as a result of the reaction of aza-Diels-Alder (Boger) with enamine followed by oxidative aromatization of the isoquinoline system [8]. 1-Morpholinocyclohexene was used as a dienophile for the first stage. Subsequent aromatization using DDQ as an oxidizing agent made it possible to successfully synthesize isoquinolines **3a**.

It should be noted that in the reaction of 3-(2-pyridyl)-1,2,4-triazine-5-carbonitriles **1b** with arynes, the corresponding isoquinolines **3b** were also obtained as main products, whereas the products of domino transformation were the minor products (the yield is not more than 3%) [9].

We also investigated the possibility of obtaining isoquinolines **3b** as a result of two-stage synthesis through the preparation of tetrahydroisoquinolines **4b**. The first step was performed by the same procedure as in the case of synthesis **4a**, and afforded the compound **4b**. However, subsequent aromatization of tetrahydrocyanoisoquinoline under various conditions, such as boiling in *o*-xylene or 4-chlorotoluene with oxidants, such as DDQ or chloranil, as well as prolonged boiling in the same high-boiling solvents in the presence of Pd/C did not lead to the formation of the desired isoquinolines **3b**. In all cases the initial tetrahydroisoquinoline **4b** was isolated. Thus, the application of this method is not acceptable for the obtaining the target 3-cyanoisoquinolines **3b**.

Thus, it was demonstrated that two mutually complementary synthetic methodologies can be used to synthesize 3-aryl, 3,4-diaryl-, as well as 3-cyano-1-(2-pyridyl)isoquinolines. Thus, in the case of R = CN (Scheme 1), the synthesis using aryne intermediates makes it possible to efficiently obtain the corresponding isoquinolines **3b**, while the method based of the preparation tetrahydroisoquinolines **4b** does not allow this because of the impossibility of subsequent aromatization by using the common methods. At the same time, in the

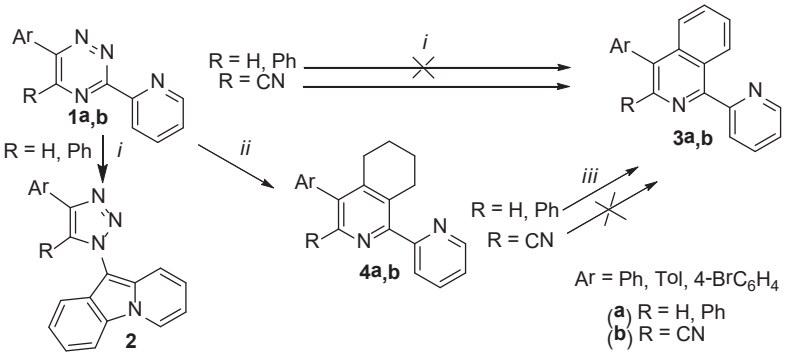

Scheme 1. Reagents and conditions: i) Anthranilic acid, isoamylnitrile, toluene — 1,4-dioxane (4: 1), boiling, 1.5 h; ii) 1-morpholinocyclohexene, without solvent, 200 °C, 4 h; iii) DDQ, *o*-xylene, 143 °C, 10 h

case of R = H or Ar, the opposite situation is observed: the synthesis of isoquinolines **3a** is possible with the use of a two-step pathway by using the corresponding enamine, and in the case of using aryl intermediates, the reaction leads mainly to rearrangement products **2**.

Experimental

NMR ^{1}H and ^{13}C spectra were recorded on the spectrometer "Bruker-Avance-400" (400 MHz), internal standard is $SiMe_4$. The melting points were measured on the "Boetius" device. Mass spectra (type of ionization is electrospray) were recorded on the device of series "MicrOTOF-Q II" of "Bruker Daltonics" (Bremen, Germany). Elemental analyses were performed on CHN analyzer PE 2400, series II by Perkin Elmer.

Acknowledgements

This work was supported by the Russian Science Foundation (Reference # 18-13-00365).

References

1. Yoshida S, Hosoya T. The Renaissance and Bright Future of Synthetic Aryne Chemistry. *Chem Lett*. 2015;44(11):1450–60. DOI: 10.1246/cl.150839.
2. Wu D, Ge H, Liu SH, Yin J. Arynes in the synthesis of polycyclic aromatic hydrocarbons. *RSC Advances*. 2013;3(45):22727–38. DOI:10.1039/C3RA43804J.
3. Miyabe H. Synthesis of Oxygen Heterocycles via Aromatic C-O Bond Formation Using Arynes. *Molecules*. 2015;20(7):12558.
4. Kopchuk DS, Nikonov IL, Khasanov AF, Giri K, Santra S, Kovalev IS, et al. Studies on the interactions of 5-R-3-(2-pyridyl)-1,2,4-triazines with arynes: inverse demand aza-Diels — Alder reaction versus aryne-mediated domino process. *Org Biomol Chem*. 2018;16(28):5119–35. DOI: 10.1039/C8OB00847G.
5. Mikata Y, Yamanaka A, Yamashita A, Yano S. Isoquinoline-Based TQEN Family as TPEN-Derived Fluorescent Zinc Sensors. *Inorganic Chemistry*. 2008;47(16):7295–301. DOI: 10.1021/ic8002614.
6. Tsuboyama A, Iwawaki H, Furugori M, Mukaide T, Kamatani J, Igawa S, et al. Homoleptic Cyclometalated Iridium Complexes with Highly Efficient Red Phosphorescence and Application to Organic Light-Emitting Diode. *J Am Chem Soc*. 2003;125(42):12971–9. DOI: 10.1021/ja034732d.
7. Nikonov IL, Kopchuk DS, Kovalev IS, Zyryanov GV, Khasanov AF, Slepukhin PA, et al. Benzyne-mediated rearrangement of 3-(2-pyridyl)-1,2,4-triazines into 10-(1H-1,2,3-triazol-1-yl)pyrido[1,2-a]indoles. *Tetrahedron Lett*. 2013;54(48):6427–9. DOI: https://doi.org/10.1016/j.tetlet.2013.09.042.
8. Kopchuk DS, Kovalev IS, Khasanov AF, Zyryanov GV, Slepukhin PA, Rusinov VL, et al. A rational protocol for the synthesis of 1-(2-pyridyl)isoquinolines. *Mendeleev Commun*. 2013;23(3):142–4. DOI: 10.1016/j.mencom.2013.05.007.
9. Kopchuk DS, Nikonov IL, Zyryanov GV, Kovalev IS, Rusinov VL, Chupakhin ON. Preparation of 3-Cyano-1-(2-Pyridyl)Isoquinolines by Using Aryne Intermediates. *Chem Heterocycl Compd*. 2014;50(6):907–10. DOI: 10.1007/s10593-014-1545-9.

Raskovalov A. A.
Chimica Techno Acta. 2018. Vol. 5, No. 3. P. 153–157.
ISSN 2409–5613

DOI: 10.15826/chimtech.2018.5.3.05

A. A. Raskovalov

Institute of High-Temperature Electrochemistry,
Ural Branch of the Russian Academy of Sciences,
20 Akademicheskaya St., Ekaterinburg, 620137, Russian Federation
E-mail: other@e1.ru

Hopping conductivity in a system with ZnS crystal lattice by non-constant force field molecular dynamics

In the paper non-constant force field molecular dynamics was used to study conductivity behavior on ZnS crystal lattice. The considered conductivity provided by electron hopping between localization centers placed randomly according to ZnS geometry. It was shown that the conductivity behavior depends on the maximal hopping distance. For the small distances the conductivity passes through the maximum around equimolar concentrations of electron donors and acceptors. Increasing in the maximal hopping distance leads to increasing in conductivity values and change shape of its concentration dependence.

Keywords: molecular dynamics; non-constant force field; polaron hopping; ZnS lattice.

Received: 08.10.2018. Accepted: 26.10.2018. Published: 31.10.2018.

Introduction

Concentration dependences of conductivity in different systems has already for a long time obtained the attention of researchers [1–3]. Such questions are often referred as percolation problems, including conductivity provided by polaron hopping between localization centers [2, 3]. At the moment a big amount of equations were suggested for describing concentration dependences of conductivity in various systems. However, analytical solutions can not account all multiplicity of factors acting on conductivity: thermal motion of ions, their mobilities, sizes and etc. An attempt to consider all microscopic picture of the conductivity process can be made with numerical methods which began to develop with progress in computer engineering. One of the most widespread methods for studying of many-boded systems on a microscopic level is molecular dynamics simulation (MD) [4, 5]. Unfortunately, classical MD can not deal with polaron hopping conductivity, because this phenomenon has quantum-mechanical nature. Early we have suggested scheme which allows including hopping conductivity into MD [6]. This approximation is possibility of particles to change their oxidation degree (and, consequently, properties and interaction laws) runtime. Thus force field becomes variable and method can be called as "Non-constant force field molecular dynamics" (NCFFMD). The method is implemented in "azTotMD" software which is available on website http://ncffmd.ru/ [7]. In our previous work we have demonstrated possibilities of the method and

the software for simulation of redox processes in liquid media [8]. The aim of the present paper is to study percolation behavior of a system with polaron hopping between localization centers placed according to ZnS crystal lattice.

Simulation details

MD simulations were performed with "azTotMD" software [7] in canonical (NVT) ensemble. Newton's equations of motion were integrated by Velocity Verlet algorithm [9] with timestep of 1 fs during 100'000 steps (0.1 ns). Equilibration time was 1 ps (1000 timesteps). Electrostatic interactions were accounted using the Ewald summation. Nosé-Hoover thermostat [10] with relaxation time of 0.2 ps was used for maintaining the temperature around 298 K. The considered system consists of electron donors (A^+), electron acceptors (A^{2+}) and counterions (X^-). The number of X^- ions was chosen equal to 500 for all studied systems. Amounts of A^+ and A^{2+} cations were given in such way to keep electroneutrality and obtain desired ratio of A^+/A^{2+} concentrations. Short range interactions were given by pair potential suggested for CuCl-$CuCl_2$ binary system [11] since solid CuCl has a ZnS structure. Initial configurations were generated with the abovementioned site [7]. The starting ion coordinates correspond to ZnS crystalline structure with some vacant sites. The box was cubic with the edge length of 25.7 Å for all studied systems. This box length roughly corresponds to a cell parameter of CuCl. The sizes of boxes was the same for simplification and, in addition, ionic radii of Cu^+ and Cu^{2+} (which are prototypes of ions A^+ and A^{2+}) are close to each other and equal to 0.77 and 0.73 Å, correspondingly [12].

For activation of electron transfer routine during the simulation value of ejump directive was set as 1 in control.txt file (one of input files for the program). The program performs electron transfer if the system decreases energy by this transfer. The difference in system energy before and after electron transfer is determined according to formula [6]:

$$\Delta U_{ij} = \sum_{k\neq i,j}\left[V_{ik}^{II} - V_{ik}^{I} + V_{jk}^{II} - V_{jk}^{I}\right] + \frac{1}{C\varepsilon}\sum_{k\neq i,j} q_k\left(\frac{q_i^{II}-q_i^{I}}{r_{ik}} + \frac{q_j^{II}-q_j^{I}}{r_{jk}}\right) + \frac{\Delta E_x}{a}\left(x_i - x_j\right), \quad (1)$$

where ΔU_{ij} is energy difference after electron transfer from i-th particle to j-th particle, V_{ik} is the Van der Waals energy of interaction between i-th and k-th particles, provided by corresponding pair potentials, q is the electric charge of the particle, r is the distance between particles, C is the constants in Coulomb's law, ε is the relative permittivity of the media, ΔE_x is the voltage drop on the X axis, a is the box length and upper indices I and II mean states of particles before and after electron transfer, correspondingly. Electronic current (I) was determined through a time derivative of difference in the number of electrons transferred in positive and negative directions:

$$I = e\frac{d\left(n^+ - n^-\right)}{dt}, \quad (2)$$

where e is the electron's charge, n^+ and n^- are the numbers of electron hops through Oyz edge in positive and negative directions along x-axis.

Results and discussion

At first let us discuss a structure of the system. The numerical experiments showed that with the presented here force field the crystal lattice is stable only in the case of the even numbers of both A^+ and A^{2+} cations. In this case one can observe crystal lattice with ZnS structure independent of the time of the system evolution, Fig. 1. One can see some vacant sites in cation sublattice, because every A^{2+} ion demands one cation vacancy to save electroneutrality. Despite of this voids the system keeps own crystal lattice right up to composition of $0.2AX{\cdot}0.8AX_2$.

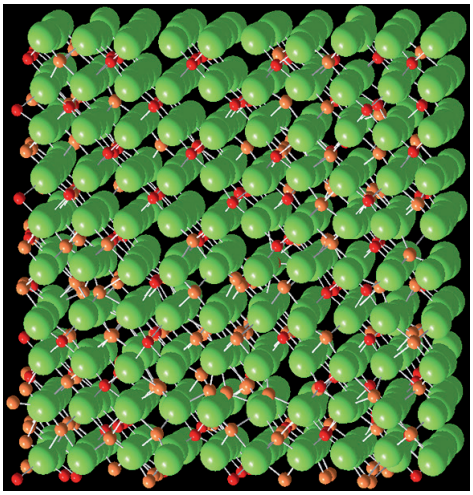

Fig. 1. The structure of the simulated system $0.5AX{\cdot}0.5AX_2$ obtained after simulation under 1V electric field during 100 000 timesteps. Big green spheres denote X^- anions, small red and orange ones — A^{2+} and A^+ cations, correspondingly

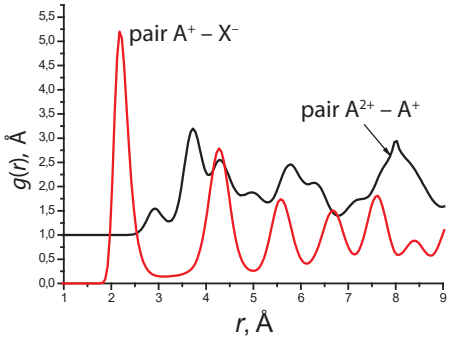

Fig. 2. The radial distribution functions, $g(r)$, of the simulated system $0.5AX{\cdot}0.5AX_2$ for A^+–X^- and A^{2+}–A^+ ion pairs

Examples of radial distribution functions (RDF) are given in Fig. 2. The RDFs are characteristic for crystalline systems; there are a number of well-resolved maxima. Distance for the first maximum determines more probable distance between ions in the first coordination sphere for a chosen pair. The position of the first maximum for A^+–A^{2+} pair does almost not depend on composition and electric field and equals to ~3.7 Å. The distance at which RDF for A^+–A^{2+} pair starts to exceed 0.1 is also almost constant and equal to ~2.7 Å. This means that if length of electron hopping is lesser than 2.7 Å, the system will not have electronic conductivity. For this reason, we set maximal hopping distance to be much higher than 2.7 Å by specifying of rElec directive in the control.txt file.

Usually, the number of electron hops through some plane is a linear function of time, Fig. 3. Without external electric field these numbers are the same for positive and negative directions, but in the case of the field the slopes of these lines differs from each other (Fig. 3). The corresponding value of current can be obtained from expression (2). Note that for observation of noticeable current we need to apply an external electric field with a colossal voltage, because current density of 1 $A{\cdot}cm^{-2}$ is approximately equal to $0.625{\cdot}10^{-9}$ single-charged particles per picosecond, per square angstrom (in units more convenient for MD). To see the noticeable number of particles for the simulation time we need to obtain high current which requires high

voltages. However, extremely high voltages can lead to the destruction of a system. In our simulations we used voltage of 1 V, higher voltages led to breaking of crystal lattice and liquid-like structure of the system.

Electronic current as a function of composition for different values of the maximal hopping distance is presented in Fig. 4. As expected, the current grows with this parameter. At small values of the distance the current passes through the maximum around $x = 0.5$. From statistical point of view the current will be maximal if probability of finding the electron acceptor (A^{2+}) near the electron donor (A^{+}) is maximal. This probability is proportional to the product of their concentrations which is maximal at $x = 0.5$. The difference of observed position of maximum from 0.5 can be caused by some reasons: asymmetry in pair potentials, different mobility of A^{+} and A^{2+} ions and etc. At high values of the maximal hopping distance the current grows with concentration of A^{+} species. This implies that if electron can hop on enough long distances the conductivity will be limited by the concentration of electron donors. In other words, if there is an electron donor, an electron acceptor always can be found. So the maximal length of the electron hop determines the shape of the concentration dependence of the conductivity.

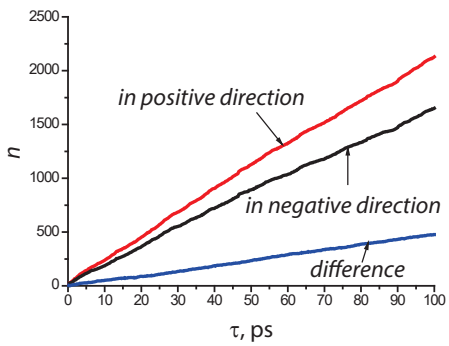

Fig. 3. The number of electron hops through the Oyz plane in positive and negative directions (and their difference) as a function of time. The simulated system is $0.5AX{\cdot}0.5AX_2$, the maximal hopping distance is 4.5 Å, the applied voltage is 1 V

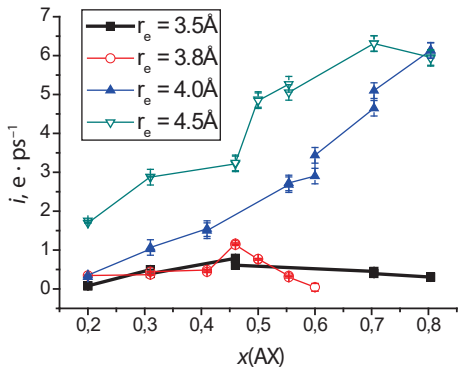

Fig. 4. Electronic current (i) as a function of composition (x) in the $xAX{-}(1{-}x)AX_2$ system under external electric field of 1 V and different maximal hopping distance (r_e)

Conclusions

Non-constant force field molecular dynamics is able to simulate electron hops between electron donors and acceptors affected by thermal movement. Thus, it is possible to study polaron conductivity of a given system by this method. In this work concentration dependence of conductivity was considered in the case of ZnS geometry for electron localization centers. It was shown that the position of the conductivity maximum depends on the maximal hopping distance.

Acknowledgements

The reported study was funded by Russian Foundation for Basic Research (RFBR), according to the research project No. 16-33-60095 mol_a_dk.

References

1. Kirkpatrick S. Percolation and Conduction. *Rev Mod Phys*. 1973; 45(4):574–88. DOI: 10.1103/RevModPhys.45.574.
2. Kurkijarvi J. Conductivity in random systems. II. Finite-size-system percolation. *Phys Rev B*. 1974; 9(15):770–4. DOI: 10.1103/PhysRevB.9.770.
3. Shklovskii BI, Éfros AL. Percolation theory and conductivity of strongly inhomogeneous media. *Sov Phys Usp*. 1975; 18(11):845–62. DOI: 10.1070/PU1975v018n11ABEH005233.
4. Allen MP, Tildesley DJ. Computer Simulation of Liquids. Oxford: Clarendon Press; 1987. 385 p.
5. Frenkel D, Smit B. Understanding Molecular Simulation From Algorithms to Applications. San Diego, California: Academic Press; 1996. 638 p.
6. Raskovalov AA. A new extension of classical molecular dynamics: an electron transfer algorithm. *J Comp Chem*. 2017; 38(5):926–32. DOI: 10.1002/jcc.24755.
7. Non-constant force field molecular dynamics. Available from: http://ncffmd.ru/set.php?lang=en (accessed: 22.02.2017).
8. Raskovalov AA, Latypov AA. Simulation of Red-Ox Reactions in Liquid Media with Non-Constant Force Field Molecular Dynamics. Rasplavy [Melts]. 2018; 6. In press. DOI: 10.1134/S0235010618060063.
9. Verlet L. Computer "Experiments" on Classical Fluids. I. Thermodynamical Properties of Lennard-Jones Molecules. *Phys Rev*. 1967; 159(1):98–103. DOI: 10.1103/PhysRev.159.98.
10. Martyna GJ, Tuckerman ME, Tobias DJ, Klein ML. Explicit Reversible Integrators for Extended Systems Dynamics. *Mol Phys*. 1996; 87(5):1117–57. DOI: 10.1080/00268979600100761.
11. Raskovalov AA, Shevelin PYu. Physico-chemical Properties of the Molten CuCl — $CuCl_2$ System: Experiment, Thermodynamics and Molecular Dynamics Simulations. *J Sol Chem*. 2018. In press. DOI: 10.1007/s10953-018-0817-x.
12. Shannon RD. Revised effective ionic radii and systematic studies of interatomic distances in halides and chalcogenides. *Acta Cryst*. 1976;A32:751–67. DOI: 10.1107/S0567739476001551.

Please note that all new submissions will be accepted in English only. Requirements for the manuscript preparation are available on the Journal's website and in the following template

Chimica Techno Acta manusctipt style guidelines (title)

A.N. Authorname[a], A.N. Authorname[b], A.N. Authorname[ab]
a Institution, address, city, country
b Institution, address, city, country
e-mail: corresponding_author@e-mail.com

Abstract

The abstract should be a single paragraph (up to 300 words) in plain text (that means — no formulae or references are permitted) that summarises the content of the article. It should set the main objectives and results of the work; giving the reader a clear idea of what has been achieved. An abstract should not be extremely short though — if yours is 1–2 sentences long, then you're not doing it right. Make sure that you use well-known, searchable terms and phrases.

Keywords: short; searchable; keywords (up to 10).

Introduction

An introduction should 'set the scene' of the work. It should clearly explain both the nature of the problem under investigation and its background. It should start off general and then focus in to the specific research question you are investigating. Ensure you include all relevant references.

Experimental (if appropiate)

Descriptions of the experiments should be provided in enough detail so that a skilled researcher is able to repeat them. Methods already published or experimental techniques already described elsewhere should be indicated by a reference. Only non-standard apparatus should be described in details; commercially available instruments are referred to by their stock numbers.

Results and discussion

This is undoubtedly the most important section of your article. It should consist of the logically ordered sequence of text, formulae, images and tables.

All formulae which appear in their own line should be numbered:

$$A = B + C \tag{1}$$

Tables should be used only when they can present information more efficiently than running text or even an image:

Table 1

Just an ordinary table without any sophisticated formatting applied

A	B	C	D
1	2	3	4
+	+	+	-

All illustrations should be of a high quality (300 dpi or higher) and should be placed in the flow of the text, not in the end of an article:

Fig. 1. Just an ordinary image

Please bear in mind that all illustrations and tables should fit smoothly within either single column (approx. 6 cm) or double column (approx. 12 cm) width.

Conclusions

Your conclusions should summarize the main paper, underline the interpretation of the key results and highlight the novelty and significance of the work. They may address some plans for relevant future work as well.

Acknowledgements (if appropiate)

All sources of funding such as grants should be declared here. Individuals who contributed to the research but are not co-authors may also be briefly acknowledged.

References

A reference should be indicated in square brackets in line with the text (e.g. [1]). The actual references in the reference list should be numbered in the order in which they appear in the text. In Chimica Techno Acta so-called Vancouver Citation Style is adopted almost as it is described in the following public domain textbook [1]:

1. Patrias K. Citing medicine: the NLM style guide for authors, editors, and publishers [Internet]. 2nd ed. Wendling DL, technical editor. Bethesda (MD): National Library of Medicine (US); 2007- [updated 2015 Oct 2; cited 2017 Jun 07]. Available from: http://www.nlm.nih.gov/citingmedicine

Note that opposed to [1] we omit the date of publication (leaving year only) of the referenced journal article, as almost all journals are continuously paginated throughout the volume. And another one — DOI or a hyperlink should always come last in a reference. These are the only major differences between our style and such described in [1], so when in doubt — you can always refer to [1], it contains tremendous number of well-organized examples.

For your convenience, below are some references to the different types of publications:

Books

2. Livingstone S. The Chemistry of Ruthenium, Rhodium, Palladium, Osmium, Iridium and Platinum. Oxford: Pergamon; 1973. 222 p.

3. Bard AJ, Faulkner LR. Electrochemical Methods: Fundamentals and Applications. 2nd ed. New York: John Wiley & Sons; 2001. 833 p.

Books not in English

4. Evdokimov AA, Efremov VA, Trunov VK, Kleyman IA, Tananaev IV. Soedineniya redkozemel'nykh elementov. Molibdaty, vol'framaty [Rare-earth elements' compounds. Molibdates, wolframates]. Moscow: Nauka; 1991. 267 p. Russian.

* Translation of the title in square brackets is not required, but highly desirable.

* For Cyrillic languages, such as Russian, please use consistent transliteration system. There are plenty, but we strongly recommend BGN/PCGN Romanization as it's one of the

easiest to read and implement (https://en.wikipedia.org/wiki/BGN/PCGN_romanization_of_Russian).

Journal articles

5. Zuev AYu, Tsvetkov DS. Oxygen nonstoichiometry, defect structure and defect-induced expansion of undoped perovskite $LaMnO_{3\pm\delta}$. Solid State Ionics. 2010;81(11–12):557–63. DOI:10.1016/j.ssi.2010.02.024

6. Shannon RD. Revised effective ionic radii and systematic studies of interatomic distances in halides and chalcogenides. Acta Cryst. 1976;A32:751–67. DOI:10.1107/S0567739476001551

7. Allred AL, Rochow EG. A scale of electronegativity based on electrostatic force. J Inorg Nucl Chem. 1958;5(4):264–8. DOI:10.1016/0022-1902(58)80003-2

* For the majority of chemical journals corresponding abbreviation is defined in Chemical Abstracts Service Source Index (CASSI, http://cassi.cas.org). If an abbreviation is not available there, please use the full name of a journal.

* Note that DOI of an article, when available, should always be provided.

Journal articles on the Internet (e.g. for online-only journals without DOI)

8. Tkach V, Nechyporuk V, Yagodynets P. Descripción matemática de la síntesis electroquímica de polímeros conductores en la presencia de surfactants. Avances en Química [Internet]. 2013[cited 2016];8(1):9–15. Spanish. Available from: http://erevistas.saber.ula.ve/index.php/avancesenquimica/article/download/6357/6168

Conference abstracts

9. Zuev AYu, Sereda VV, Malyshkin DA, Ivanov IL, Tsvetkov DS. Mechano-chemical coupling in double perovskites as energy related materials. In: Abstracts of the XX Mendeleev Congress on general and applied chemistry, Vol. 3; 2016 Sep 26–30; Ekaterinburg, Russia. p. 325.

10. Steparuk AS, Usachev SA, Tsvetkov DS, Sosnovskikh VYa, Zuev AYu. Novyy katodnyy material na osnove mayenita dlya elektrokhimicheskogo karboksilirovaniya organicheskikh soedineniy [New mayenite-based cathode material for electrochemical carboxylation of organic compounds]. In: Tezisy dokladov XXVI Rossiyskoy molodezhnoy nauchnoy konferentsii "Problemy teoreticheskoy i eksperimental'noy khimii" [Abstracts of XXVI Russian scientific conference for young scientists "Problems of theoretical and experimental chemistry"]; 2016 Apr 27–29; Ekaterinburg, Russia. p. 285–286. Russian.

Dissertations

11. ten Donkelaar SFP. Development of Stable Oxygen Transport Membranes [dissertation]. Enschede (The Netherlands): University of Twente; 2015. 140 p.

Patents

12. Chemezov OV, Batukhtin VP, Apisarov AP, Isakov AV, Zaikov YuP, inventors; Institute of High-Temperature Electrochemistry UB RAS, assignee. Sposob polucheniya nano- i mikrovolokon kremniya elektrolizom dioksida kremniya iz rasplavov soley. Russian Federation patent RU 2427526. 2011 Aug 27. Russian.

13. Menta E, Da Re G, Grugni M., authors; Cti Europe S.R.L., assignee. Derivatives of chromen-2-one as inhibitors of vegf production in mammalian cells. United States patent US20060122387 A1. 2006 Jun 8.

Chimica Techno Acta

Учредитель — Уральский федеральный университет имени первого Президента России Б. Н. Ельцина
620002, Россия, Екатеринбург, ул. Мира, 19

Редактор *Е. Е. Крамаревская*
Художник-оформитель *Е. Р. Даурова*
Верстальщик *В. К. Матвеев*

Свидетельство о регистрации
ПИ № ФС77-56172 от 15.11.2013

Адрес журнала:
Россия, 620000,
Екатеринбург, ул. Мира, 28, оф. Х-268
E-mail: t.a.pospelova@urfu.ru
Формат 70×100/16. Заказ № 321.
Тираж 500 экз.
Отпечатано в типографии
Издательско-полиграфического центра УрФУ
620000, Екатеринбург, ул. Тургенева, 4
Тел.: +7 (343) 350-56-64, 350-90-13
Факс: +7 (343) 358-93-06
E-mail: press-urfu@mail.ru

Founded by Ural Federal University named after
the first President of Russia B. N. Yeltsin
19, Mira St., Ekaterinburg, 620002, Russia

Journal Registration Certificate
PI № FS 77-56172 as of 15.11.2013

Principal Contact
Office X-268, Mira Str.,
620000, Ekaterinburg, Russia
E-mail: t.a.pospelova@urfu.ru

Format 70×100/16.
Circulation 500 cop.

Publisher — Ural Federal University
Publishing Centre
4, Turgenev St., 620000 Ekaterinburg, Russia
Phone: +7 343 350 56 64, +7 343 350 90 13
Fax: +7 343 358 93 06
E-mail: press-urfu@mail.ru